Kalman-Bucy Filter-Based Tracking Controller Design and Experimental Validations for a Quadcopter with Parametric Uncertainties and Disturbances

ZHU Xuan-Zhi[a], David Cabecinhas[a], Wei Xie[b*] , Pedro Casau[c], Carlos Silvestre[d†], Pedro Batista[a,c] and Paulo Oliveira[a,e]

[a] Institute for Systems and Robotics, Laboratory for Robotics and Engineering Systems, Instituto Superior Técnico, Universidade de Lisboa, Lisboa, Portugal.
[b] Department of Automation, Shanghai Jiao Tong University, Shanghai, China.
[c] Department of Electrical and Computer Engineering, Instituto Superior Técnico, Universidade de Lisboa, Lisboa, Portugal.
[d] Department of Electrical and Computer Engineering, University of Macau, Macau, China.
[e] Associated Laboratory for Energy, Transports and Aeronautics, Institute of Mechanical Engineering, Instituto Superior Técnico, Universidade de Lisboa, Lisboa, Portugal.

ARTICLE HISTORY
Compiled April 21, 2022

ABSTRACT
This paper addresses the problem of trajectory tracking for a quadcopter subject to parametric uncertainties and disturbances. Using the backstepping technique and assuming known parametric uncertainties and disturbances, a nominal controller is proposed for the quadcopter. In order to ensure that the controller is adaptive to parametric uncertainties (i.e., unknown but constant mass and moment of inertia) and external disturbances, an exponentially stable estimator is designed based on the Kalman-Bucy filter. The interconnected closed-loop system of the plant, the controller, and the estimator is such that the backstepping error is uniformly ultimately bounded. Furthermore, simulation and experimental results are presented, validating the stability and robustness properties of the proposed control strategy.

KEYWORDS
Quadcopter; adaptive control; backstepping; Kalman-Bucy filter; estimator

1. Introduction

Motion control of quadcopters has become a hot research topic in recent years due to their promising applications in both military and civilian fields. For instance, they have been widely used in search, surveillance, mapping, and rescue mission in hazardous environments that impede direct human intervention. These small-scale vehicles demonstrate many favorable characteristics, such as easy maintenance, hovering capability, vertical take-off and landing (VTOL) capability, and low cost, making them highly versatile and maneuverable test platforms. Among different motion control tasks, the focus of this paper is on the basic problem of trajectory tracking for a quadcopter

∗CONTACT Wei Xie: weixie@sjtu.edu.cn
† On leave from the Instituto Superior Técnico, Universidade de Lisboa, Lisboa, Portugal.

subject to certain parametric uncertainties, which involves the design of control laws that steer the vehicle to follow a time parameterized reference.

The dynamics of a quadcopter inherit: (a) nonlinearity; (b) underactuation; (c) parametric uncertainty; and (d) external disturbances. (a) and (b) make it difficult to control quadcopters in general. To cope with (a), linear controllers, e.g., Castillo, Lozano, and Dzul (2005); Hoffmann, Huang, Waslander, and Tomlin (2007), were proposed but only guarantee local stability with restrictive region of attraction and usually depend on linearization around certain operating point. They are popular and among the first controllers developed for quadcopters. Being aware of such limitation, nonlinear controllers have been developed to achieve a wider flight envelope with more general tracking trajectories, e.g., backstepping control Bouabdallah and Siegwart (2005); Madani and Benallegue (2006), sliding mode control Xu and Özgüner (2006), and feedback linearization Lee, Kim, and Sastry (2009). Since the controllers above parametrize the orientation of the quadcopter in Euler angles, they exhibit singularities when representing complex rotational maneuvers. Meanwhile, the proposed nonlinear control laws are often discontinuous or time-varying due to (b), which prevents the existence of any time-invariant feedback control law by violation of Brockett's condition Brockett et al. (1983). Notably, by parametrizing the orientation of the quadcopter in the Special Orthogonal Group of order 3 and embracing Brockett's condition, a singularity-free time-invariant nonlinear controller was proposed in Aguiar and Hespanha (2007) that is able to globally drive a quadcopter to an arbitrary small neighborhood of a position reference. Furthermore, most of the aforementioned controllers rely on accurate dynamical models, but (c) can hinder their performance and robustness properties. Indeed, the presence of (c) and/or (d) is inescapable in realistic application scenarios. On one hand, it is not always possible to accurately measure/identify dynamical model parameters (e.g., mass, moment of inertia), especially in tasks where payload changes. On the other hand, quadcopters are sensitive to external disturbances such as wind gusts due to their small size and weight.

To mitigate the effects of uncertain parameters and external disturbances, adaptive control and other robust control strategies were proposed by a few works and achieve different levels of stability, adaptivity, and robustness in the problem of trajectory tracking for a quadcopter. In terms of the underlying adaption scheme, the proposed strategies fall into the following categories: (a) estimation of parametric uncertainties in Dydek, Annaswamy, and Lavretsky (2013); Islam, Liu, and El Saddik (2014); Wang, Song, Huang, and Tang (2016); (b) estimation of quadcopter states (position, linear velocity, attitude, etc.) by nonlinear deterministic filters in Hua and Allibert (2018), by Kalman-type filters in Barrau and Bonnabel (2017), by geometric stochastic filter in Hashim, Abouheaf, and Abido (2021); and (c) both in Aguiar and Hespanha (2007). In this paper, we are given estimates of the quadcopter states with relatively low noise level, enabled by an indoor motion capture system (to be introduced later). Our interest is to perform (a), namely online parameter identification of a controlled quadcopter, which suffers from parametric uncertainties (mass, moment of inertia, and external disturbances) and may be subject to certain Gaussian noise in its dynamics. While most of the related works rely on a suitable adaptation law to achieve adaptivity or robustness, the underlying design is coupled with that of the control law. Moreover, the adaption law therein is derived via accommodating negative time derivative of a Lyapunov function along solutions, with no guarantees that the estimates converge to the actual parameter values. Moreover, consideration of both inertia uncertainties (mass and moment of inertia) and external disturbances is absent in Aguiar and Hespanha (2007); Cabecinhas, Cunha, and Silvestre (2014); Fang and Gao (2012); Huang,

Xian, Diao, Yang, and Feng (2010); Lee et al. (2009); Mellinger, Lindsey, Shomin, and Kumar (2011); Mukherjee and Waslander (2012); Pounds, Bersak, and Dollar (2012); Wang, Nahon, and Trentini (2014); Zeng et al. (2011). In particular, the works Fang and Gao (2012); Huang et al. (2010); Pounds et al. (2012); Wang et al. (2014) assume constant moment of inertia with yet varying mass, which is conceptually unacceptable. It is worth mentioning that a parameter estimator that considers both inertia uncertainties and external disturbances is designed on top of a backstepping controller in Cabecinhas, Batista, Oliveira, and Silvestre (2018) for trajectory tracking control of a 2-D hovercraft. However, the persistent of excitation condition therein is not sufficient for asymptotic stability of their parameter estimator and hence the stability analysis lacks rigor. Nevertheless, it offers inspiration on how we approach a solution to the trajectory tracking problem for a 3-D quadcopter, which brings more challenges since the controller should be designed carefully to meet time-critical flight tasks.

Taking into account the aforementioned aspects, this paper takes advantage of the backstepping technique in Aguiar and Hespanha (2007) and the parameter estimator design in Cabecinhas et al. (2018). Specifically, we consider a quadcopter with unknown but constant mass, moment of inertia, and external force disturbances, for which an adaptive backstepping controller is proposed consisting of a backstepping controller and a parameter estimator that exponentially recovers unknown parameters. In this way, we extend the results in Aguiar and Hespanha (2007) by separating the controller design and the estimator design, while we extend the results in Cabecinhas et al. (2018) by designing exponentially convergent cascaded Kalman-Bucy filters for recovery of unknown parameters of a 3-D quadcopter. Comparing to other control methods, the reasons for using a backstepping controller are threefold: (a) enlargement of the region of attraction compared to linear controller or linearization methods; (b) free of chattering phenomenon as often happens in sliding mode control; (c) avoidance of dynamic extension which can lead to singularity in feedback linearization control. Because the plant dynamics are linear with respect to the unknown parameters, some natural choices of the parameter estimator can be considered: least-squares Mellinger et al. (2011), gradient descent Wang et al. (2014), Kalman-Bucy filter. Comparing to the former two methods, the Kalman-Bucy filter not only suffers no singularity issues but also has the following advantages: (a) emulation-like design of the adaptive backstepping controller: a nominal controller is first designed without considering the unknown parameters, afterwards, we take into account the effects induced by the latter and we derive an appropriate persistence-of-excitation condition to ensure stability for the obtained system, as in the works Aguiar and Hespanha (2007); Cabecinhas et al. (2018). This adds flexibility on controller design and simplicity in estimator design; (b) guarantees of exponentially convergent estimates: the stability analysis of both the open-loop and the closed-loop estimator leverages on solid stability analysis on the Kalman-Bucy filter Kalman and Bucy (1961) and perturbed Kalman-Bucy filter Viegas, Batista, Oliveira, and Silvestre (2016); (c) optimality: the Kalman-Bucy filter is the optimal minimum mean-square error estimator when the process noise and the observation noise are zero-mean Gaussian random processes.

One of the difficulties in the course of our controller design is the occurrence of singularities in the control law if one directly inverts the estimates, which can lead to unbounded control signals. Fortunately, by using a cascaded Kalman-Bucy filter, one is able to eliminate those singularities, where the newly added filter provides estimates of parameter inverses. Another difficulty in this pursuit lies in finding the persistent of excitation condition for exponential convergence of the parameter estimator. We handle this issue by studying uniform complete observability for a linear time-varying

system generated by the quadcopter dynamics and arriving at concrete conditions for persistence of excitation, which is closely related to richness of control signals. The other difficulty is the stability proof of the interconnected system consisting of the plant, the backstepping controller, and the parameter estimator, for which we resort to Lyapunov analysis. Although our proposed control scheme guarantees sound theoretical results, the following challenges remain: the persistent of excitation condition should be verified, and the initial estimation errors should be small enough. To solve the former problem, we verify *a posteriori* the persistent of excitation condition in a case-dependent manner. To solve this problem completely, one may turn to model predictive control in order to pick in an *online* manner the control signals that fulfill the persistent of excitation condition. As for the latter problem, we suggest two solutions: to obtain good initial estimates or to wait for some time until the open-loop parameter estimator approaches sufficiently close to the actual parameters and then close the loop.

Compared to the aforementioned works on adaptive and/or robust backstepping control, the main contributions of this paper are:

1. a novel adaptive backstepping controller for trajectory tracking of a quadcopter by coupling a backstepping controller and cascaded Kalman-Bucy filters. In fact, by first designing a nominal controller assuming no modeling uncertainty then feeding the unknown parameters with convergent estimates, we are using a control scheme referred in the literature as self-tuning control Slotine, Li, et al. (1991). For the interconnected system consisting of the plant and the controller, we show ultimate boundedness of backstepping errors if the persistent of excitation condition holds, which is closely related to richness of control signals. Nevertheless, few works have simultaneously proposed this control strategy and proved its stability;
2. a singularity-free time-invariant continuous control law obtained by cascading two Kalman-Bucy filters that attain inverse of unknown parameters, as opposed to Fang and Gao (2012); Huang et al. (2010); Islam et al. (2014); Wang et al. (2016), whose controllers suffer from singularities due to linearization or dynamic extension or parameter inversion;
3. design of an exponentially stable parameter estimator that recovers the unknown parameters while allowing one to tune their convergence rates through the associated noise covariance matrices, as opposed to Aguiar and Hespanha (2007); Benrezki, Tayebi, and Tadjine (2018); Cabecinhas et al. (2014); Fang and Gao (2012); Huang et al. (2010), which consider only some but not all of these parameters and have little implication of how the convergence rate may be tuned;
4. validation of the proposed control scheme through simulation and experimental runs in terms of: practical stability of the interconnected system, exponential stability of the parameter estimator, and robustness against endogenous disturbance (mass, moment of inertia, and external force disturbances) as well as exogenous disturbance (white Gaussian noises).

The remainder of the paper is organized as follows. Notations and the parameter estimator design for a general linear-in-parameters system are introduced in Section 2. The quadcopter dynamical model and the control objective are presented in Section 3. Section 4 focuses on the development of a nominal backstepping controller. Section 5 and Section 6 analyze the stability of the interconnected system in an open-loop and closed-loop manner, separately. Simulation results are presented in Section 7. Section

8 and Section 9 shows the experimental setup and results, respectively. Section 10 summarizes the paper and describes potential future work.

2. Mathematical Preliminaries

2.1. Notations

Let $\mathbb{R}$ denote the real field, $\mathbb{R}_{\geq 0} := [0, \infty)$, $\mathbb{R}_{>0} := (0, \infty)$, $\mathbb{Z}_{>0} := \{1, 2, \dots\}$. The Euclidean n-space is denoted by $\mathbb{R}^n$, endowed with the inner product $\langle \mathbf{x}, \mathbf{y} \rangle := \mathbf{x}^\top \mathbf{y}$ for every $\mathbf{x}, \mathbf{y} \in \mathbb{R}^n$ and the Euclidean norm $\|\mathbf{x}\| := \sqrt{\langle \mathbf{x}, \mathbf{x} \rangle}$ for every $\mathbf{x} \in \mathbb{R}^n$. Given a vector $\mathbf{x} \in \mathbb{R}^n$ and some $i \in \mathbb{Z}_{>0}$, x_i denotes its i-th component. Given a matrix $\mathbf{A} \in \mathbb{R}^{n \times m}$ and some $i, j \in \mathbb{Z}_{>0}$, a_{ij} denotes the entry of $\mathbf{A}$ on the i-th row and j-th column. The identity matrix of order n is denoted by $\mathbf{I}_n$, the zero matrix of size $n \times m$ is denoted by $\mathbf{0}_{n \times m}$, and the n-dimensional vector whose each component is 1 is denoted by $\mathbf{1}_n$. The symbol $\mathbf{e}_i$ denotes a unit vector of appropriate dimension whose i-th component is 1. For every vector $\mathbf{x} \in \mathbb{R}^n$, define the function $\operatorname{diag} : \mathbb{R}^n \to \mathbb{R}^{n \times n}$ as $\operatorname{diag}(\mathbf{x}) := [x_1 \mathbf{e}_1 \; x_2 \mathbf{e}_2 \; \cdots \; x_n \mathbf{e}_n]$. For every matrix $\mathbf{A} \in \mathbb{R}^{n \times m}$, let $\operatorname{Null}(\mathbf{A}) := \{\mathbf{x} \in \mathbb{R}^m : \mathbf{A}\mathbf{x} = \mathbf{0}_{n \times 1}\}$ denote its null space. Given an $n \times n$ real symmetric matrix $\mathbf{A}$, let its n real eigenvalues be arranged such that $\lambda_1(\mathbf{A}) \geq \lambda_2(\mathbf{A}) \geq \cdots \geq \lambda_n(\mathbf{A})$. A function $\mathbf{f} : \mathcal{X} \to \mathbb{R}^m$ with $\mathcal{X} \subset \mathbb{R}^n$ is of class $\mathcal{C}^k$ if all of its partial derivatives up through order k exist and are continuous. The Special Orthogonal group of order 3 is $\mathsf{SO}(3) := \left\{\mathbf{R} \in \mathbb{R}^{3 \times 3} : \mathbf{R}^\top \mathbf{R} = \mathbf{I}_3, \det(\mathbf{R}) = 1\right\}$, whose Lie Algebra is $\mathfrak{so}(3) := \{\mathbf{M} \in \mathbb{R}^{3 \times 3} : \mathbf{M} = -\mathbf{M}^\top\}$ together with the Lie bracket $[\mathbf{X}, \mathbf{Y}] := \mathbf{X}\mathbf{Y} - \mathbf{Y}\mathbf{X}$ for every $\mathbf{X}, \mathbf{Y} \in \mathfrak{so}(3)$. The operator $\mathbf{S} : \mathbb{R}^3 \to \mathfrak{so}(3)$ defines the isomorphism between the algebras $(\mathbb{R}^3, \cdot \times \cdot)$ and $(\mathfrak{so}(3), [\cdot, \cdot])$ satisfying

$$\mathbf{S}(\mathbf{x})\mathbf{y} := \mathbf{x} \times \mathbf{y} \tag{1}$$

for every $\mathbf{x}, \mathbf{y} \in \mathbb{R}^3$.

2.2. Parameter estimator background

Since Kalman-Bucy filtering plays an important role in this paper, we present below the framework adopted for parameter estimation. A generic nonlinear dynamical system can be represented by the differential equation

$$\dot{\mathbf{x}} = \mathbf{f}_0(\mathbf{x}, \boldsymbol{\xi}, t), \tag{2}$$

where $\mathbf{x} \in \mathbb{R}^n$ is the state, $\boldsymbol{\xi} \in \mathbb{R}^m$ is the unknown parameter, and $\mathbf{f}_0 : \mathbb{R}^n \times \mathbb{R}^m \times \mathbb{R}_{\geq 0} \to \mathbb{R}^n$. We say that (2) is linear-in-parameters if it can be written as

$$\dot{\mathbf{x}} = \mathbf{A}_0(\mathbf{x}, t)\boldsymbol{\xi} + \mathbf{b}_0(\mathbf{x}, t), \tag{3}$$

where the continuous bounded function $\mathbf{A}_0 : \mathbb{R}^n \times \mathbb{R}_{\geq 0} \to \mathbb{R}^{n \times m}$ and the bounded continuous function $\mathbf{b}_0 : \mathbb{R}^n \times \mathbb{R}_{\geq 0} \to \mathbb{R}^n$. Assuming that the solution to (3) is a continuous bounded function on $\mathbb{R}_{\geq 0}$ and that the unknown parameter $\boldsymbol{\xi}$ is constant,

we define the following system

$$\begin{aligned} \dot{\mathbf{x}} &= \mathbf{A}_{\boldsymbol{\xi}}(t)\boldsymbol{\xi} + \mathbf{b}_{\boldsymbol{\xi}}(t), \\ \dot{\boldsymbol{\xi}} &= \mathbf{0}_{m\times 1}, \end{aligned} \tag{4}$$

where the continuous functions $\mathbf{A}_{\boldsymbol{\xi}} : \mathbb{R}_{\geq 0} \to \mathbb{R}^{n\times m}$ and $\mathbf{b}_{\boldsymbol{\xi}} : \mathbb{R}_{\geq 0} \to \mathbb{R}^n$. Assuming full state measurement, we have that

$$\mathbf{y} = \mathbf{x}, \tag{5}$$

where $\mathbf{y} \in \mathbb{R}^n$ is the state measurement.

By augmenting the state to include the unknown parameters, the system (4) with output equation (5) can be written as a linear time-varying system as follows

$$\begin{aligned} \dot{\boldsymbol{\zeta}} &= \mathbf{A}_{\boldsymbol{\zeta}}(t)\boldsymbol{\zeta} + \mathbf{b}_{\boldsymbol{\zeta}}(t), \\ \mathbf{y} &= \mathbf{C}_{\boldsymbol{\zeta}}\boldsymbol{\zeta}, \end{aligned} \tag{6}$$

where $\boldsymbol{\zeta} := [\mathbf{x}^\top \ \boldsymbol{\xi}^\top]^\top \in \mathbb{R}^{n+m}$, $\mathbf{A}_{\boldsymbol{\zeta}}(t) := \begin{bmatrix} \mathbf{0}_{n\times n} & \mathbf{A}_{\boldsymbol{\xi}}(t) \\ \mathbf{0}_{m\times n} & \mathbf{0}_{m\times m} \end{bmatrix}$, $\mathbf{b}_{\boldsymbol{\zeta}}(t) := \begin{bmatrix} \mathbf{b}_{\boldsymbol{\xi}}(t) \\ \mathbf{0}_{m\times 1} \end{bmatrix}$, and $\mathbf{C}_{\boldsymbol{\zeta}} := \begin{bmatrix} \mathbf{I}_n & \mathbf{0}_{n\times m} \end{bmatrix}$. Noticing that $\mathbf{A}_{\boldsymbol{\zeta}}$ is nilpotent, with $\mathbf{A}_{\boldsymbol{\zeta}}^k = \mathbf{0}_{(n+m)\times(n+m)}$ for $k \geq 2$, we compute the transition matrix $\boldsymbol{\Phi}$ associated with $\mathbf{A}_{\boldsymbol{\zeta}}$ through the Peano-Baker series as

$$\boldsymbol{\Phi}(t, t_0) = \mathbf{I}_{n+m} + \int_{t_0}^{t} \mathbf{A}_{\boldsymbol{\zeta}}(\tau)d\tau = \begin{bmatrix} \mathbf{I}_n & \int_{t_0}^{t} \mathbf{A}_{\boldsymbol{\xi}}(\tau)d\tau \\ \mathbf{0}_{m\times n} & \mathbf{I}_m \end{bmatrix}, \tag{7}$$

where $t_0, t \in \mathbb{R}_{\geq 0}$.

Given the linear structure of (6), we choose a Kalman-Bucy filter to be the parameter estimator, described by

$$\begin{aligned} \dot{\widehat{\boldsymbol{\zeta}}} &= \mathbf{A}_{\boldsymbol{\zeta}}(t)\widehat{\boldsymbol{\zeta}} + \mathbf{b}_{\boldsymbol{\zeta}}(t) + \mathbf{K}_{\boldsymbol{\zeta}}\left(\mathbf{y} - \mathbf{C}_{\boldsymbol{\zeta}}\widehat{\boldsymbol{\zeta}}\right), \\ \mathbf{K}_{\boldsymbol{\zeta}} &= \mathbf{P}_{\boldsymbol{\zeta}}\mathbf{C}_{\boldsymbol{\zeta}}^\top\mathbf{R}_{\boldsymbol{\zeta}}^{-1}, \\ \dot{\mathbf{P}}_{\boldsymbol{\zeta}} &= \mathbf{A}_{\boldsymbol{\zeta}}(t)\mathbf{P}_{\boldsymbol{\zeta}} + \mathbf{P}_{\boldsymbol{\zeta}}\mathbf{A}_{\boldsymbol{\zeta}}^\top(t) + \mathbf{Q}_{\boldsymbol{\zeta}} - \mathbf{P}_{\boldsymbol{\zeta}}\mathbf{C}_{\boldsymbol{\zeta}}^\top\mathbf{R}_{\boldsymbol{\zeta}}^{-1}\mathbf{C}_{\boldsymbol{\zeta}}\mathbf{P}_{\boldsymbol{\zeta}}, \end{aligned} \tag{8}$$

where $\widehat{\boldsymbol{\zeta}} := [\widehat{\mathbf{x}}^\top \ \widehat{\boldsymbol{\xi}}^\top]^\top \in \mathbb{R}^{n+m}$ is the estimate, and the positive definite symmetric matrix $\mathbf{R}_{\boldsymbol{\zeta}} \in \mathbb{R}^{n\times n}$ and the positive semidefinite symmetric matrix $\mathbf{Q}_{\boldsymbol{\zeta}} \in \mathbb{R}^{(n+m)\times(n+m)}$ are respectively the so-called measurement noise covariance matrix and process noise covariance matrix. The initial conditions for (8) are such that $\widehat{\boldsymbol{\zeta}}(t_0) \in \mathbb{R}^{n+m}$ and $\mathbf{P}_{\boldsymbol{\zeta}}(t_0) \in \mathbb{R}^{(n+m)\times(n+m)}$ is symmetric and positive definite. Defining $\widetilde{\boldsymbol{\zeta}} := \boldsymbol{\zeta} - \widehat{\boldsymbol{\zeta}}$ as the estimation error, the interconnected system consisting of (6) and (8) can be written as

$$\begin{aligned} \dot{\widetilde{\boldsymbol{\zeta}}} &= \left(\mathbf{A}_{\boldsymbol{\zeta}}(t) - \mathbf{K}_{\boldsymbol{\zeta}}\mathbf{C}_{\boldsymbol{\zeta}}\right)\widetilde{\boldsymbol{\zeta}}, \\ \mathbf{K}_{\boldsymbol{\zeta}} &= \mathbf{P}_{\boldsymbol{\zeta}}\mathbf{C}_{\boldsymbol{\zeta}}^\top\mathbf{R}_{\boldsymbol{\zeta}}^{-1}, \\ \dot{\mathbf{P}}_{\boldsymbol{\zeta}} &= \mathbf{A}_{\boldsymbol{\zeta}}(t)\mathbf{P}_{\boldsymbol{\zeta}} + \mathbf{P}_{\boldsymbol{\zeta}}\mathbf{A}_{\boldsymbol{\zeta}}^\top(t) + \mathbf{Q}_{\boldsymbol{\zeta}} - \mathbf{P}_{\boldsymbol{\zeta}}\mathbf{C}_{\boldsymbol{\zeta}}^\top\mathbf{R}_{\boldsymbol{\zeta}}^{-1}\mathbf{C}_{\boldsymbol{\zeta}}\mathbf{P}_{\boldsymbol{\zeta}}. \end{aligned} \tag{9}$$

To facilitate the analysis on stability of the system (9), we introduce the observability Grammian associated with the pair $(\mathbf{A}_{\boldsymbol{\zeta}}, \mathbf{C}_{\boldsymbol{\zeta}})$

$$\mathbf{W}(t_0, t_1) := \int_{t_0}^{t_1} \boldsymbol{\Phi}^\top(\tau, t_0)\mathbf{C}_{\boldsymbol{\zeta}}^\top \mathbf{R}_{\boldsymbol{\zeta}}^{-1}\mathbf{C}_{\boldsymbol{\zeta}}\boldsymbol{\Phi}(\tau, t_0)d\tau \tag{10}$$

for every $t_0, t_1 \in \mathbb{R}_{\geq 0}$, where $\boldsymbol{\Phi}$ is defined in (7) and $\mathbf{R}_{\boldsymbol{\zeta}}$ is defined in (8). Meanwhile, we borrow from Viegas et al. (2016) the notion of uniform complete observability for a general linear time-varying system and particularize this concept to (6).

Definition 2.1. Given the system (6) with an initial time $t_0 \in \mathbb{R}_{\geq 0}$, the pair $(\mathbf{A}_{\boldsymbol{\zeta}}, \mathbf{C}_{\boldsymbol{\zeta}})$ is said to be uniformly completely observable (UCO) if and only if there exist constants $\Delta t, \chi \in \mathbb{R}_{>0}$ such that

$$\chi^{-1} \leq \mathbf{d}^\top \mathbf{W}(t, t + \Delta t)\mathbf{d} \leq \chi \tag{11}$$

for every $t \geq t_0$ and every unit vector $\mathbf{d} \in \mathbb{R}^{n+m}$, where $\mathbf{W}$ is defined in (10).

The following lemma provides a sufficient condition for exponential stability of the system (9).

Lemma 2.2. *Consider the system* (6) *with an initial time* $t_0 \in \mathbb{R}_{\geq 0}$. *If there exists* $\epsilon, \Delta t \in \mathbb{R}_{>0}$ *such that for every* $t \geq t_0$ *and every unit vector* $\mathbf{c} \in \mathbb{R}^m$,

$$\left\| \int_t^\tau \mathbf{A}_{\boldsymbol{\xi}}(\sigma)\mathbf{c}d\sigma \right\| \geq \epsilon \tag{12}$$

for some $\tau \in [t, t + \Delta t]$, *then the estimate* $\widehat{\boldsymbol{\zeta}}$ *of the Kalman-Bucy filter* (8) *converges globally exponentially to the state* $\boldsymbol{\zeta}$ *of the system* (6).

Proof. Please refer to Appendix A. □

In the proof above, we invoke the results of (Jazwinski, 1970, Theorem 7.4) and (Bucy & Joseph, 1968, Theorem 5.4) to conclude exponential stability of the system (9). In these works, the system to be estimated is a stochastic one, but the proofs therein can be adapted to the deterministic case since the homogeneous part of the filter equation therein is in the same form as that of (9). Furthermore, we point out that the proofs therein contain an error in the bounds for the error covariance matrix and have been corrected in Delyon (2001). One may argue the absence of uniform complete controllability (UCC) in the proof above for exponential stability of the Kalman-Bucy filter, as often appears in the literature, e.g. (Batista, Silvestre, & Oliveira, 2011, Theorem 4). However, using similar arguments above leads to the fact that the pair $(\mathbf{A}_{\boldsymbol{\zeta}}, \mathbf{D}_{\boldsymbol{\zeta}})$ is UCC by taking $\mathbf{D}_{\boldsymbol{\zeta}} = \mathbf{I}_{n+m}$. This is obvious in the parameter estimator equation (8), where the evolution of $\dot{\mathbf{P}}_{\boldsymbol{\zeta}}$ is originally governed by $\dot{\mathbf{P}}_{\boldsymbol{\zeta}} = \mathbf{A}_{\boldsymbol{\zeta}}(t)\mathbf{P}_{\boldsymbol{\zeta}} + \mathbf{P}_{\boldsymbol{\zeta}}\mathbf{A}_{\boldsymbol{\zeta}}^\top(t) + \mathbf{D}_{\boldsymbol{\zeta}}\mathbf{Q}_{\boldsymbol{\zeta}}\mathbf{D}_{\boldsymbol{\zeta}}^\top - \mathbf{P}_{\boldsymbol{\zeta}}\mathbf{C}_{\boldsymbol{\zeta}}^\top\mathbf{R}_{\boldsymbol{\zeta}}^{-1}\mathbf{C}_{\boldsymbol{\zeta}}\mathbf{P}_{\boldsymbol{\zeta}}$.

2.3. Technical lemmas

We present below some lemmas which help with the proof of our main results. The first lemma studies perturbations of a symmetric matrix.

Lemma 2.3. *Let $\mathbf{K}, \widetilde{\mathbf{K}} \in \mathbb{R}^{n\times n}$ be two symmetric matrices, then*

$$\lambda_{i+j-n}(\mathbf{K}+\widetilde{\mathbf{K}}) \geq \lambda_i(\mathbf{K}) + \lambda_j(\widetilde{\mathbf{K}}), \tag{13}$$

where $i, j \in \{1, 2, \ldots, n\}$.

Proof. Please refer to, for instance, Weyl (1912). □

The next lemma studies continuity the eigenvalues of a matrix with respect to the entries of the matrix.

Lemma 2.4. *Let $\mathbf{K}_1, \mathbf{K}_2 \in \mathbb{R}^{n\times n}$, then there exists a permutation τ of $\{1, 2, \ldots, n\}$ such that*

$$\max_{1\leq j\leq n} \left|\lambda_j(\mathbf{K}_1) - \lambda_{\tau(j)}(\mathbf{K}_2)\right| \leq 2^{\frac{2n-1}{n}} (\|\mathbf{K}_1\| + \|\mathbf{K}_2\|)^{\frac{n-1}{n}} \|\mathbf{K}_1 - \mathbf{K}_2\|^{\frac{1}{n}}, \tag{14}$$

where $\|\cdot\|$ denotes the maximum singular value of a matrix.

Proof. Please refer to, for instance, (Horn & Johnson, 2012, Theorem D2). □

The following lemma studies the asymptotic behavior of a particular class of functions, which is the core in the proof of our main results.

Lemma 2.5. *Let $U : \mathbb{R}^n \times \mathbb{R}_{\geq 0} \to \mathbb{R}$ be defined by*

$$U(\mathbf{x}, t) = -\sigma_2(t) \|\mathbf{x}\|^2 + \sigma_1(t) \|\mathbf{x}\| + \sigma_3(t) \|\mathbf{x}\|^3, \tag{15}$$

where $\sigma_i : \mathbb{R}_{\geq 0} \to \mathbb{R}$ for each $i \in \{0, 1, 2, 3\}$ satisfy

$$\lim_{t\to\infty} \sigma_0(t) = 0, \tag{16}$$

$$\sigma_1(t) = \max\{\Sigma_1, \sigma_0(t)\}, \tag{17}$$

$$\lim_{t\to\infty} \sigma_2(t) = \Sigma_2, \tag{18}$$

$$\lim_{t\to\infty} \sigma_3(t) = 0 \tag{19}$$

with $\Sigma_1, \Sigma_2 > 0$. Then there exist $T, c > 0$ and $0 < a < b$ such that

$$U(\mathbf{x}, t) \leq -c \|\mathbf{x}\|^2 \tag{20}$$

for every $t \geq T$ and every $\mathbf{x}$ such that $a \leq \|\mathbf{x}\| \leq b$.

Proof. Please refer to Appendix B. □

3. Control Objective

The quadcopter, depicted in Fig. 1, is modeled as a rigid body in 3-dimensional space. Consider a fixed inertial frame $\{I\}$ and a body frame $\{B\}$ attached to the quadcopter's center of mass. The configuration of $\{B\}$ with respect to $\{I\}$ belongs to $\mathsf{SO}(3)$.

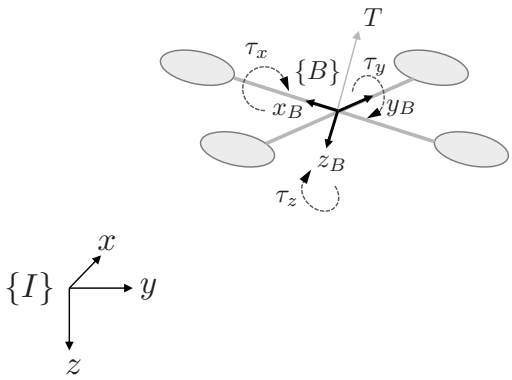

Figure 1. Sketch of quadcopter plant with indication of reference frames and thrust forces.

Following the formalization in Castillo et al. (2005), the kinematics and dynamics of the quadcopter are given by

$$\begin{aligned}
\dot{\mathbf{p}} &= \mathbf{R}\mathbf{v}, \\
\dot{\mathbf{R}} &= \mathbf{R}\mathbf{S}(\boldsymbol{\omega}), \\
\dot{\mathbf{v}} &= -\mathbf{S}(\boldsymbol{\omega})\mathbf{v} + g\mathbf{R}^\top \mathbf{e}_3 + m^{-1}\mathbf{R}^\top \mathbf{b} - m^{-1}T\mathbf{e}_3, \\
\dot{\boldsymbol{\omega}} &= -\mathbf{J}^{-1}\mathbf{S}(\boldsymbol{\omega})\mathbf{J}\boldsymbol{\omega} + \mathbf{J}^{-1}\boldsymbol{\tau},
\end{aligned} \tag{21}$$

where $\mathbf{p} \in \mathbb{R}^3$ is the position in $\{I\}$, $\mathbf{R} \in \mathsf{SO}(3)$ is the rotation matrix that maps vectors in $\{B\}$ to $\{I\}$, $\mathbf{v} \in \mathbb{R}^3$ is the linear velocity in $\{B\}$, $\mathbf{S} : \mathbb{R}^3 \to \mathfrak{so}(3)$ maps vectors in $\mathbb{R}^3$ to 3-by-3 skew-symmetric matrices, $\boldsymbol{\omega} \in \mathbb{R}^3$ is the angular velocity in $\{B\}$, $g \in \mathbb{R}_{>0}$ is the local gravitational acceleration constant, $m \in \mathbb{R}_{>0}$ is the mass constant, $\mathbf{b} \in \mathbb{R}^3$ is the constant external force disturbances in $\{I\}$, $T \in \mathbb{R}$ is the thrust acting on the quadcopter's center of mass, $\mathbf{J} \in \mathbb{R}^{3\times 3}$ is the constant moment of inertia, and $\boldsymbol{\tau} \in \mathbb{R}^3$ is the torque. A common assumption on $\mathbf{J}$ is widely adopted in the literature as follows:

Assumption 1. The moment of inertia is such that $\mathbf{J} = \mathrm{diag}(\mathbf{j})$, where $j_i \in \mathbb{R}_{>0}$ for each $i \in \{1, 2, 3\}$.

In fact, for a general 3-dimensional body, it is *always* possible to choose the body frame $\{B\}$ such that its moment of inertia is a diagonal matrix. Satisfaction of Assumption 1 demonstrates both theoretical and practical advantages. For theoretical consideration, Assumption 1 enables a linear representation of the moment of inertia in the plant dynamics, and hence facilitates the use of Kalman-Bucy filtering. This point will be clear in the sequel. For practical consideration, Assumption 1 holds if and only if the body frame $\{B\}$ is the principal axes of inertia. With uniform density distribution and symmetric geometry of the quadcopter, the body frame can be chosen as three orthogonal axes of symmetry located at the center point of symmetry. When the moment of inertia is not diagonal, one may either reselect the body frame $\{B\}$ until the moment of inertia becomes diagonal, or turn to other filtering techniques such as nonlinear filtering and geometric filtering since it is difficult to arrive at a linear representation of the moment of inertia in the plant dynamics.

In order to have a final system with a linear dependency on the unknown param-

eters (whose concept will be defined explicitly later), define the following constant parameters

$$\begin{aligned}
\xi_1 &:= m^{-1} \in \mathbb{R}, \\
\boldsymbol{\xi}_2 &:= m^{-1}\mathbf{b} \in \mathbb{R}^3, \\
\boldsymbol{\xi}_3 &:= [(j_2 - j_3)j_1^{-1} \ (j_3 - j_1)j_2^{-1} \ (j_1 - j_2)j_3^{-1}]^\top \in \mathbb{R}^3, \\
\boldsymbol{\xi}_4 &:= [j_1^{-1} \ j_2^{-1} \ j_3^{-1}]^\top \in \mathbb{R}^3, \\
\boldsymbol{\Xi}_4 &:= \operatorname{diag}(\boldsymbol{\xi}_4) = \mathbf{J}^{-1} \in \mathbb{R}^{3\times 3}
\end{aligned} \tag{22}$$

so that (21) can be rewritten as

$$\begin{aligned}
\dot{\mathbf{p}} &= \mathbf{R}\mathbf{v}, \\
\dot{\mathbf{R}} &= \mathbf{R}\mathbf{S}(\boldsymbol{\omega}), \\
\dot{\mathbf{v}} &= -\mathbf{S}(\boldsymbol{\omega})\mathbf{v} + g\mathbf{R}^\top \mathbf{e}_3 + \mathbf{R}^\top \boldsymbol{\xi}_2 - \xi_1 T \mathbf{e}_3, \\
\dot{\boldsymbol{\omega}} &= \boldsymbol{\Omega}(\boldsymbol{\omega})\boldsymbol{\xi}_3 + \mathbf{U}(\boldsymbol{\tau})\boldsymbol{\xi}_4
\end{aligned} \tag{23}$$

with

$$\begin{aligned}
\boldsymbol{\Omega}(\boldsymbol{\omega}) &:= \operatorname{diag}\left([\omega_2\omega_3 \ \omega_1\omega_3 \ \omega_1\omega_2]^\top\right), \\
\mathbf{U}(\boldsymbol{\tau}) &:= \operatorname{diag}(\boldsymbol{\tau}),
\end{aligned} \tag{24}$$

where $\mathbf{p}$, $\mathbf{R}$, $\mathbf{v}$, and $\boldsymbol{\omega}$ the plant states, and T and $\boldsymbol{\tau}$ the inputs.

Given a reference trajectory $\mathbf{p}_d : \mathbb{R}_{\geq 0} \to \mathbb{R}^3$ of at least class $\mathcal{C}^3$ with bounded time derivatives $\dot{\mathbf{p}}_d$, $\ddot{\mathbf{p}}_d$, and $\dddot{\mathbf{p}}_d$ that are defined on $\mathbb{R}_{\geq 0}$, we call $\mathbf{p}_d$, $\dot{\mathbf{p}}_d$, $\ddot{\mathbf{p}}_d$, and $\dddot{\mathbf{p}}_d$ the reference signals. Based on the definitions above, the control objective is stated as follows:

Problem 1. For the quadcopter (21) with unknown constant mass m, moment of inertia $\mathbf{J}$, and external force disturbances $\mathbf{b}$, devise a feedback control law such that each plant state, input, and reference signal (possibly except $\mathbf{p}$, $\mathbf{p}_d$) is bounded, the position tracking error $t \mapsto \|\mathbf{p}(t) - \mathbf{p}_d(t)\|$ is uniformly ultimately bounded, and the unknown parameters m, $\mathbf{J}$, and $\mathbf{b}$ are exponentially recovered.

In fact, our proposed method, to be specified in the following, can be easily extended to consider deterministic nonconstant parameters and/or disturbances that follow linear time-varying dynamics, by taking advantage of Kalman-Bucy filtering. For generic deterministic nonconstant parameters and/or disturbances, one may turn to adding extra robustness terms in the Lyapunov function to enforce noise rejection. However, this goes beyond our current control objective.

4. Nominal Controller

This section focuses on the trajectory tracking controller design for the quadcopter assuming known mass, moment of inertia, and external force disturbances, which is referred to as the nominal controller. Define the position tracking error, in the inertial

frame, as

$$\mathbf{z}_1 := \mathbf{p} - \mathbf{p}_d, \tag{25}$$

whose time derivative is

$$\dot{\mathbf{z}}_1 = \mathbf{R}\mathbf{v} - \dot{\mathbf{p}}_d. \tag{26}$$

Choose the first Lyapunov candidate function

$$V_1 := \frac{1}{2}\alpha \mathbf{z}_1^\top \mathbf{z}_1 \tag{27}$$

for some $\alpha \in \mathbb{R}_{>0}$, which is used in the proofs but plays no role in defining the feedback control law. The time derivative of (27) along the solution to (26) yields

$$\dot{V}_1 = \alpha \mathbf{z}_1^\top (\mathbf{R}\mathbf{v} - \dot{\mathbf{p}}_d), \tag{28}$$

where $\mathbf{v}$ can be viewed as a virtual control input to make $\dot{V}_1$ negative, which can be achieved by setting $\mathbf{v}$ equal to $-k_1\mathbf{R}^\top \mathbf{z}_1 + \mathbf{R}^\top \dot{\mathbf{p}}_d$ for some $k_1 \in \mathbb{R}_{>0}$. To accomplish this goal, define the linear velocity error as

$$\mathbf{z}_2 := \mathbf{v} + k_1\mathbf{R}^\top \mathbf{z}_1 - \mathbf{R}^\top \dot{\mathbf{p}}_d - \boldsymbol{\delta}, \tag{29}$$

that we would like to drive to zero, where we introduce the constant $\boldsymbol{\delta} \in \mathbb{R}^3 \backslash \{\mathbf{0}_{3\times 1}\}$ to avoid violating Brockett's condition Brockett et al. (1983); Oriolo and Nakamura (1991) at the expense of controlling the linear velocity at $\boldsymbol{\delta}$ distance away from $-k_1\mathbf{R}^\top \mathbf{z}_1 + \mathbf{R}^\top \dot{\mathbf{p}}_d$. Now, the closed-loop expression of (28) becomes

$$\dot{V}_1 := -\alpha k_1 \mathbf{z}_1^\top \mathbf{z}_1 + \alpha \mathbf{z}_1^\top \mathbf{R}(\mathbf{z}_2 + \boldsymbol{\delta}). \tag{30}$$

The time derivative of $\mathbf{z}_2$ is given by

$$\dot{\mathbf{z}}_2 = \mathbf{S}(\mathbf{z}_2 + \boldsymbol{\delta})\boldsymbol{\omega} - \xi_1 T \mathbf{e}_3 + \mathbf{h}(\cdot) \tag{31}$$

with

$$\mathbf{h}(\mathbf{z}_1, \mathbf{z}_2, \mathbf{R}, \ddot{\mathbf{p}}_d) := -k_1^2 \mathbf{R}^\top \mathbf{z}_1 + k_1(\mathbf{z}_2 + \boldsymbol{\delta}) + g\mathbf{R}^\top \mathbf{e}_3 - \mathbf{R}^\top \ddot{\mathbf{p}}_d + \mathbf{R}^\top \boldsymbol{\xi}_2. \tag{32}$$

Consider the second Lyapunov candidate function

$$V_2 := V_1 + \frac{1}{2}\mathbf{z}_2^\top \mathbf{z}_2. \tag{33}$$

The time derivative of V_2 along the solution to (26) and (31) is

$$\dot{V}_2 = -\alpha k_1 \mathbf{z}_1^\top \mathbf{z}_1 + \alpha \mathbf{z}_1^\top \mathbf{R}(\mathbf{z}_2 + \boldsymbol{\delta}) + \mathbf{z}_2^\top \left(\mathbf{D}\boldsymbol{\mu} + \mathbf{h}(\cdot)\right), \tag{34}$$

where the constant matrix $\mathbf{D} := [-\xi_1 \mathbf{e}_3 \ \mathbf{S}(\boldsymbol{\delta})]$ and the vector $\boldsymbol{\mu} := [T \ \boldsymbol{\omega}^\top]^\top$. In (34), we deviate from the deduction in Aguiar and Hespanha (2007) by separating the term $\alpha \mathbf{z}_1^\top \mathbf{R}^\top \mathbf{z}_2$ from the term $\mathbf{z}_2^\top \left(\mathbf{D}\boldsymbol{\mu} + \mathbf{h}(\cdot)\right)$, as motivated by Xie, Cabecinhas, Cunha,

and Silvestre (2019), in order to asymptotically stabilize the error $\mathbf{z}_2$ around the origin. This will be made clear in the proof of Lemma 4.2. To proceed, we first present a lemma that asserts full rank of the matrix $\mathbf{D}$ by a suitable choice of $\boldsymbol{\delta}$.

Lemma 4.1. *The matrix* $\mathbf{D}$ *defined in* (34) *has full rank for every* $\boldsymbol{\delta} = [\delta_1 \ \delta_2 \ \delta_3]^\top$ *satisfying* $\delta_3 \neq 0$. *Moreover,* $\mathbf{D}_r := \mathbf{D}^\top \left(\mathbf{D}\mathbf{D}^\top\right)^{-1}$ *is a right inverse of* $\mathbf{D}$.

Proof. This proof resembles that of (Aguiar & Hespanha, 2007, Property 1). $\mathbf{D}$ has full rank if there exists a 3-by-3 submatrix of $\mathbf{D}$ having nonzero determinant. Consider the submatrix formed by the first three columns of $\mathbf{D}$, i.e.,

$$\begin{bmatrix} 0 & 0 & -\delta_3 \\ 0 & \delta_3 & 0 \\ -\xi_1 & -\delta_2 & \delta_1 \end{bmatrix}, \tag{35}$$

whose determinant is $-\xi_1\delta_3^2$. Therefore, $\mathbf{D}$ has full rank if δ_3 is nonzero. There are other possible choices of a 3-by-3 submatrix of $\mathbf{D}$, but they lead to additional constraints on $\boldsymbol{\delta}$. As a result, a right inverse of $\mathbf{D}$ can be chosen to be $\mathbf{D}_r := \mathbf{D}^\top \left(\mathbf{D}\mathbf{D}^\top\right)^{-1}$ that is well-defined and satisfies $\mathbf{D}\mathbf{D}_r = \mathbf{I}_3$. □

Remark 1. Note that the fulfillment of the condition in Lemma 4.1 implies that $\text{Null}(\mathbf{D}) = \{[0 \ \lambda\boldsymbol{\delta}^\top]^\top : \lambda \in \mathbb{R}, \delta_3 \neq 0\}$.

With such observation, we are allowed to define

$$\boldsymbol{\mu}_d(\mathbf{z}_1, \mathbf{z}_2, \mathbf{R}, \ddot{\mathbf{p}}_d, t) := \mathbf{D}_r(-\mathbf{h}(\cdot) - k_2\mathbf{z}_2) + \gamma(t)\boldsymbol{\mu}_{\mathbf{D}} \tag{36}$$

for some $k_2 \in \mathbb{R}_{>0}$, arbitrary $\boldsymbol{\mu}_{\mathbf{D}} \in \text{Null}(\mathbf{D})$, and arbitrary bounded function $\gamma : \mathbb{R}_{\geq 0} \to \mathbb{R}$ of class $\mathcal{C}^1$ with bounded derivative. By setting $\boldsymbol{\mu}$ in (34) to $\boldsymbol{\mu}_d$, we zero out the term $\mathbf{D}\boldsymbol{\mu} + \mathbf{h}(\cdot)$ in (34) and introduce negative definite term $-k_2\mathbf{z}_2^\top\mathbf{z}_2$ therein.

Observe that the first component of the vector $\boldsymbol{\mu}$ is the input T and thus we can set

$$T(\mathbf{z}_1, \mathbf{z}_2, \mathbf{R}, \ddot{\mathbf{p}}_d) := \begin{bmatrix} 1 & \mathbf{0}_{1\times 3} \end{bmatrix} \boldsymbol{\mu}_d(\cdot), \tag{37}$$

where T is independent of t since $\begin{bmatrix} 1 & \mathbf{0}_{1\times 3} \end{bmatrix} \gamma(t)\boldsymbol{\mu}_{\mathbf{D}} = 0$ (see Remark 1). Further calculation reveals that (37) can be rewritten as

$$T(\mathbf{z}_1, \mathbf{z}_2, \mathbf{R}, \ddot{\mathbf{p}}_d) := -\xi_1^{-1}\delta_3^{-1}\boldsymbol{\delta}^\top\mathbf{h}_{\mathbf{D}}(\cdot), \tag{38}$$

where $\mathbf{h}_{\mathbf{D}}(\mathbf{z}_1, \mathbf{z}_2, \mathbf{R}, \ddot{\mathbf{p}}_d) := -\mathbf{h}(\cdot) - k_2\mathbf{z}_2$. We use the remaining components of $\boldsymbol{\mu}$, namely $\boldsymbol{\omega}$, to form the angular velocity error

$$\mathbf{z}_3 := \boldsymbol{\omega} - \begin{bmatrix} \mathbf{0}_{3\times 1} & \mathbf{I}_3 \end{bmatrix} \boldsymbol{\mu}_d(\cdot). \tag{39}$$

With T defined in (38) and $\mathbf{z}_3$ defined in (39), the closed-loop form (34) can be written as

$$\dot{V}_2 = -\alpha k_1 \mathbf{z}_1^\top\mathbf{z}_1 + \alpha\mathbf{z}_1^\top\mathbf{R}(\mathbf{z}_2 + \boldsymbol{\delta}) - k_2\mathbf{z}_2^\top\mathbf{z}_2 + \mathbf{z}_2^\top\mathbf{S}(\boldsymbol{\delta})\mathbf{z}_3. \tag{40}$$

The time derivative of $\mathbf{z}_3$, with T defined in (38), is computed as

$$\dot{\mathbf{z}}_3 = \boldsymbol{\Omega}(\boldsymbol{\omega})\boldsymbol{\xi}_3 + \boldsymbol{\Xi}_4\boldsymbol{\tau} - \begin{bmatrix}\mathbf{0}_{3\times 1} & \mathbf{I}_3\end{bmatrix}\dot{\boldsymbol{\mu}}_d(\cdot), \tag{41}$$

where $\dot{\boldsymbol{\mu}}_d$ denotes the time derivative of $\boldsymbol{\mu}_d$. We introduce the third Lyapunov candidate function

$$V_3 := V_2 + \frac{1}{2}\beta\mathbf{z}_3^\top\mathbf{z}_3 \tag{42}$$

for some $\beta \in \mathbb{R}_{>0}$, with its time derivative along the solution to (26), (31), and (41), and with T defined in (38), given by

$$\begin{aligned}\dot{V}_3 = &-\alpha k_1\mathbf{z}_1^\top\mathbf{z}_1 + \alpha\mathbf{z}_1^\top\mathbf{R}(\mathbf{z}_2+\boldsymbol{\delta}) - k_2\mathbf{z}_2^\top\mathbf{z}_2 \\ &+ \beta\mathbf{z}_3^\top\big(\boldsymbol{\Omega}(\boldsymbol{\omega})\boldsymbol{\xi}_3 + \boldsymbol{\Xi}_4\boldsymbol{\tau} - [\mathbf{0}_{3\times 1}\,\mathbf{I}_3]\dot{\boldsymbol{\mu}}_d(\cdot) - \beta^{-1}\mathbf{S}(\boldsymbol{\delta})\mathbf{z}_2\big).\end{aligned} \tag{43}$$

In order to cancel the terms $\boldsymbol{\Omega}(\boldsymbol{\omega})\boldsymbol{\xi}_3$, $\begin{bmatrix}\mathbf{0}_{3\times 1} & \mathbf{I}_3\end{bmatrix}\dot{\boldsymbol{\mu}}_d(\cdot)$, and $\beta^{-1}\mathbf{S}(\boldsymbol{\delta})\mathbf{z}_2$, select the control law for $\boldsymbol{\tau}$ as

$$\boldsymbol{\tau}(\mathbf{z}_1,\mathbf{z}_2,\mathbf{z}_3,\mathbf{R},\ddot{\mathbf{p}}_d,t) := \boldsymbol{\Xi}_4^{-1}\big(-k_3\mathbf{z}_3 - \boldsymbol{\Omega}(\boldsymbol{\omega})\boldsymbol{\xi}_3 + \begin{bmatrix}\mathbf{0}_{3\times 1} & \mathbf{I}_3\end{bmatrix}\dot{\boldsymbol{\mu}}_d(\cdot) + \beta^{-1}\mathbf{S}(\boldsymbol{\delta})\mathbf{z}_2\big) \tag{44}$$

for some $k_3 \in \mathbb{R}_{>0}$, where $\boldsymbol{\omega}$ can be written in terms of $\mathbf{z}_1$, $\mathbf{z}_2$, $\mathbf{z}_3$, $\mathbf{R}$, $\ddot{\mathbf{p}}_d$, and t in virtue of (39). Then, the time derivative of V_3 along (26), (31), and (41), with T defined in (38) and $\boldsymbol{\tau}$ defined in (44), becomes

$$\dot{V}_3 = -\alpha k_1\mathbf{z}_1^\top\mathbf{z}_1 + \alpha\mathbf{z}_1^\top\mathbf{R}(\mathbf{z}_2+\boldsymbol{\delta}) - k_2\mathbf{z}_2^\top\mathbf{z}_2 - \beta k_3\mathbf{z}_3^\top\mathbf{z}_3. \tag{45}$$

Now, we are ready to present the stability result.

Lemma 4.2. *Under Assumption 1, choose $\boldsymbol{\delta}$ such that $\delta_3 \neq 0$. Given a reference trajectory $\mathbf{p}_d : \mathbb{R}_{\geq 0} \to \mathbb{R}^3$ of at least class $\mathcal{C}^3$ with bounded time derivatives $\dot{\mathbf{p}}_d$, $\ddot{\mathbf{p}}_d$, and $\dddot{\mathbf{p}}_d$, consider the plant* (21) *driven by the control laws* (38) *and* (44)*. For every initial condition in $\mathbb{R}^3 \times \mathsf{SO}(3) \times \mathbb{R}^6$, the solution to* (21) *exists; $\mathbf{v}$, $\boldsymbol{\omega}$, T, and $\boldsymbol{\tau}$ are bounded on $\mathbb{R}_{\geq 0}$; $t \mapsto \mathbf{z}_1(t)$ is uniformly ultimately bounded by $2k_1^{-1}\|\boldsymbol{\delta}\|$, $\mathbf{z}_2(t) \to \mathbf{0}_{3\times 1}$ and $\mathbf{z}_3(t) \to \mathbf{0}_{3\times 1}$ as $t \to \infty$.*

Proof. Please refer to Appendix C. □

5. Open-loop Design of the Parameter Estimator

Consider the system that consists of the parameter estimator in open-loop with the plant (21) driven by the control laws (38) and (44). The parameter estimator has access to the state and input information, but its output, namely the estimated parameter, is not allowed to enter the rest of the system. Such a configuration serves as our first attempt to approach the control objective. The parameter estimator design is separated into two phases, as detailed in the sequel. It is noted that each signal in (21) can be viewed as a bounded continuous function on $\mathbb{R}_{\geq 0}$ by virtue of Lemma 4.2.

5.1. Estimator for $\boldsymbol{\xi_1}$, $\boldsymbol{\xi_2}$, $\boldsymbol{\xi_3}$, and $\boldsymbol{\xi_4}$

Rewriting the plant dynamics (23) in the form of (4), we obtain

$$\mathbf{A}_{\boldsymbol{\xi}}(t) = \begin{bmatrix} -T(t)\mathbf{e}_3 & \mathbf{R}^\top(t) & \mathbf{0}_{3\times 3} & \mathbf{0}_{3\times 3} \\ \mathbf{0}_{3\times 1} & \mathbf{0}_{3\times 3} & \boldsymbol{\Omega}(\boldsymbol{\omega}(t)) & \mathbf{U}(\boldsymbol{\tau}(t)), \end{bmatrix} \tag{46}$$

which is bounded and continuous on $\mathbb{R}_{\geq 0}$, and

$$\mathbf{b}_{\boldsymbol{\xi}}(t) = \begin{bmatrix} \mathbf{S}(\boldsymbol{\omega}(t))\mathbf{v}(t) + g\mathbf{R}^\top(t)\mathbf{e}_3 \\ \mathbf{0}_{3\times 1} \end{bmatrix} \tag{47}$$

which is bounded and continuous on $\mathbb{R}_{\geq 0}$. Before proceeding, let us make an assumption that will guarantee global exponential stability of the estimation error system by direct application of Lemma 2.2.

Assumption 2. Given $t_0 \in \mathbb{R}_{\geq 0}$, there exists $\epsilon, \Delta t \in \mathbb{R}_{>0}$ such that for every $t \geq t_0$ and every unit vector $\mathbf{c} := [c_1^\top \ \mathbf{c}_2^\top \ \mathbf{c}_3^\top \ \mathbf{c}_4^\top]^\top \in \mathbb{R}^{10}$,

$$\left\| \int_t^\tau \begin{bmatrix} -T(\sigma)\mathbf{e}_3 c_1 + \mathbf{R}^\top(\sigma)\mathbf{c}_2 \\ \boldsymbol{\Omega}(\boldsymbol{\omega}(\sigma))\mathbf{c}_3 + \mathbf{U}(\boldsymbol{\tau}(\sigma))\mathbf{c}_4 \end{bmatrix} d\sigma \right\| \geq \epsilon \tag{48}$$

for some $\tau \in [t, t + \Delta t]$.

Assumption 2 essentially states that the signals should be sufficiently rich throughout time to conclude global exponential stability of the estimation error system, which can be achieved in practice by choice of an appropriate reference trajectory. To facilitate understanding "richness" of signals, let us consider the following trivial example. Suppose the reference signals $\mathbf{p}_d(t) = \dot{\mathbf{p}}_d(t) = \ddot{\mathbf{p}}_d(t) = \dddot{\mathbf{p}}_d(t) = \mathbf{0}_{3\times 1}$ for every $t \in \mathbb{R}_{\geq 0}$ and the quadcopter is initialized as $\mathbf{p} = \mathbf{v} = \boldsymbol{\omega} = \mathbf{0}_{3\times 1}$, $\mathbf{R} = \mathbf{I}_3$. Selecting $\mathbf{b} = \mathbf{0}_{3\times 1}$, $\gamma(t) \equiv 0$, $\boldsymbol{\delta} = \delta_3 \mathbf{e}_3$, then under open-loop design of the parameter estimator, we obtain analytic solutions to the equations of motion (21) as[1]:

$$\mathbf{p}(t) = \begin{cases} (-\delta_3 t e^{-kt} - \dfrac{\delta_3}{k} e^{-kt} + \dfrac{\delta_3}{k})\mathbf{e}_3, & \text{if } k_1 = k_2 = k \\ (\alpha_1 e^{-0.5\lambda_1 t} + \alpha_2 e^{-0.5\lambda_2 t} + \dfrac{\delta_3}{k_1})\mathbf{e}_3, & \text{if } k_1 \neq k_2 \end{cases} \tag{49}$$

$$\mathbf{v}(t) = \begin{cases} k\delta_3 t e^{-kt}\mathbf{e}_3, & \text{if } k_1 = k_2 = k \\ (-0.5\alpha_1\lambda_1 e^{-0.5\lambda_1 t} - 0.5\alpha_2\lambda_2 e^{-0.5\lambda_2 t})\mathbf{e}_3, & \text{if } k_1 \neq k_2 \end{cases} \tag{50}$$

$$\boldsymbol{\omega}(t) = \mathbf{0}_{3\times 1} \tag{51}$$

$$\mathbf{R}(t) = \mathbf{I}_3 \tag{52}$$

for every $t \in \mathbb{R}_{\geq 0}$. If we select the unit vector $\mathbf{c}$ in (48) such that $c_1 = 0$, $\mathbf{c}_2 = \mathbf{c}_4 = \mathbf{0}_{3\times 1}$, then the left-hand side of the inequality becomes *zero* for any $\tau \in [t, t + \Delta t]$, which is absurd since $\epsilon > 0$. Hence for this artificial case where the reference signals are not *rich* enough and when the quadcopter is perfectly initialized, the assumption above fails to hold. But in practice, the external disturbances $\mathbf{b}$ are not identically zero, and even if they do, we can select a non-constant function γ and a more generic

[1] $\lambda_1 = k_1 + k_2 + |k_1 - k_2|$, $\lambda_2 = k_1 + k_2 - |k_1 - k_2|$, $\alpha_1 = \frac{\lambda_2 \delta_3}{2k_1|k_1 - k_2|}$, $\alpha_2 = -\frac{\lambda_1 \delta_3}{2k_1|k_1 - k_2|}$

$\boldsymbol{\delta}$ to generate rich signals. Furthermore, we have not closed the loop by feeding the nominal controller with the estimates coming from the parameter estimator. When we close the loop in the next section, both the assumption here and the solutions to the equations of motion here will take a slightly different form. Hence it remains to detect whether the closed-loop system of this example satisfies Assumption 2.

Remark 2. We present in Appendix E a program that can be used to detect numerically satisfaction or violation of the premise of Lemma 2.2 (and hence Assumption 2). Due to numerical verification, the drawbacks of this program are clear: numerical integration of the integrand in (48); finite samples of the unit vector $\mathbf{c}$; finite samples of the lower limit of the integral, namely t. However, the results that will be presented in Section 7 show versatility and usefulness of this program. In particular, we present in Section 7.1 a sanity check of the program for the specific example (49)-(52), which shows violation of Assumption 2.

Remark 3. Assumption 2 is a stronger version compared to that of (Cabecinhas et al., 2018, Lemma 2) ensuring complete observability. The latter asks for linear independence of columns of $\int_t^\tau \mathbf{A}_{\boldsymbol{\xi}}(\sigma)d\sigma$ as functions on $[t, t+\Delta t]$, which relaxes the condition (12) by allowing the dependence of ϵ on a chosen t. In that case, stability of the Kalman-Bucy filter is guaranteed but attractivity may not be.

A naive straightforward application of this estimator in closed-loop with (38) and (44) can lead to singularities due to the use of parameter inverses in the control laws, i.e., ξ_1^{-1} in (38) and $\boldsymbol{\Xi}_4^{-1}$ in (44). To eliminate singularities, we propose a cascaded estimator for the parameter inverses, detailed in the sequel.

5.2. Estimator for $\boldsymbol{\xi_1^{-1}}$ and $\boldsymbol{\Xi_4^{-1}}$

It is clear from (22) that $\xi_1^{-1} = m$ and $\boldsymbol{\Xi}_4^{-1} = \mathbf{J} = \mathrm{diag}(\mathbf{j})$. We will first derive an estimator for m as follows.

Considering the following linear system that describes the dynamics of m,

$$\begin{aligned} \dot{m} &= 0, \\ y_m &= \xi_1 m \equiv 1, \end{aligned} \tag{53}$$

where y_m is the output, we arrive at the following set of equations describing the Kalman-Bucy filter for (53):

$$\begin{aligned} \dot{\widehat{m}} &= k_m \left(y_m - \xi_1 \widehat{m}\right), \\ k_m &= r_m^{-1} \xi_1 p_m, \\ \dot{p}_m &= q_m - r_m^{-1} \xi_1^2 p_m^2, \end{aligned} \tag{54}$$

where $\widehat{m} \in \mathbb{R}$ is the mass estimate, $r_m \in \mathbb{R}_{>0}$ and $q_m \in \mathbb{R}_{\geq 0}$ are tuning gains. Initial conditions for (54) are such that $\widehat{m}(t_0) \in \mathbb{R}$ and $p_m(t_0) \in \mathbb{R}_{>0}$. In practice, however,

ξ_1 is not known. This fact motivates to construct the following set of equations:

$$\begin{aligned}\dot{\widehat{m}} &= k_m\left(y_m - \widehat{\xi}_1\widehat{m}\right),\\ k_m &= r_m^{-1}\widehat{\xi}_1 p_m,\\ \dot{p}_m &= q_m - r_m^{-1}\widehat{\xi}_1^2 p_m^2,\end{aligned} \tag{55}$$

where ξ_1 in (54) is replaced with its estimate $\widehat{\xi}_1$ coming from the estimator in Section 5.1, whose stability is studied in the following lemma.

Lemma 5.1. *Under Assumption 2, consider the system* (55)*. The estimation error* $t \mapsto \widetilde{m}(t) := m - \widehat{m}(t)$ *converges globally exponentially to* 0 *as* t *goes to infinity.*

Proof. Under Assumption 2, we have that $t \mapsto \widetilde{\xi}_1(t)$ converges exponentially to 0 as t goes to infinity. Therefore, (55) can be seen as a perturbed Kalman-Bucy filter for (54) in the sense of Viegas et al. (2016) and the stability property remains. □

The estimator design for $\mathbf{j}$ follows similar lines and is omitted for the sake of simplicity. The estimate of $\mathbf{j}$ is denoted by $\widehat{\mathbf{j}}$ and the estimate for $\boldsymbol{\Xi}_4^{-1}$ can be retrieved by the operation diag $(\widehat{\mathbf{j}})$. The corresponding estimation error is defined by $t \mapsto \widetilde{\mathbf{j}}(t) := \mathbf{j} - \widehat{\mathbf{j}}(t)$, which converges globally exponentially to $\mathbf{0}$ as t goes to infinity by virtue of Lemma 5.1.

6. Closed-loop Design of the Parameter Estimator

To ease the notational burden, let $\boldsymbol{\xi} := [\xi_1\ \boldsymbol{\xi}_2^\top\ \boldsymbol{\xi}_3^\top\ \boldsymbol{\xi}_4^\top]^\top$ and $\boldsymbol{\eta} := [m\ \mathbf{j}^\top]^\top$ denote the parameters, $\widehat{\boldsymbol{\xi}}$ and $\widehat{\boldsymbol{\eta}}$ denote the estimates from the parameter estimator, and $\widetilde{\boldsymbol{\xi}} := \boldsymbol{\xi} - \widehat{\boldsymbol{\xi}}$ and $\widetilde{\boldsymbol{\eta}} := \boldsymbol{\eta} - \widehat{\boldsymbol{\eta}}$ denote the estimation errors.

In this section, we consider that our controller has no access to the actual values of the parameters. Rather, these parameters are replaced by their estimates obtained from the parameter estimators, leading to modified control laws. In the sequel, we use the accent symbol $\widehat{(\cdot)}$ to denote modified functions for which $\boldsymbol{\xi}$ and $\boldsymbol{\eta}$ are replaced $\widehat{\boldsymbol{\xi}}$ and $\widehat{\boldsymbol{\eta}}$. The modified control law for the thrust is

$$\widehat{T}(\mathbf{z}_1, \mathbf{z}_2, \mathbf{R}, \ddot{\mathbf{p}}_d, \widehat{\boldsymbol{\xi}}, \widehat{\boldsymbol{\eta}}) := -\widehat{m}\delta_3^{-1}\boldsymbol{\delta}^\top \widehat{\mathbf{h}}_{\mathbf{D}}(\cdot), \tag{56}$$

where $\widehat{m}$ comes from the estimator in Section 5.2 and replaces ξ_1^{-1} in (38). The modified control law for the torque is

$$\widehat{\boldsymbol{\tau}}(\mathbf{z}_1, \mathbf{z}_2, \widehat{\mathbf{z}}_3, \mathbf{R}, \ddot{\mathbf{p}}_d, t, \widehat{\boldsymbol{\xi}}, \widehat{\boldsymbol{\eta}}, \dot{\widehat{\boldsymbol{\xi}}}) := \widehat{\mathbf{J}}\big(- k_3\widehat{\mathbf{z}}_3 - \boldsymbol{\Omega}(\boldsymbol{\omega})\widehat{\boldsymbol{\xi}}_3 + [\mathbf{0}_{3\times 1}\ \mathbf{I}_3]\widehat{\boldsymbol{\mu}}_d(\cdot) + \beta^{-1}\mathbf{S}(\boldsymbol{\delta})\mathbf{z}_2\big), \tag{57}$$

where $\widehat{\mathbf{J}} := \text{diag}(\widehat{\mathbf{j}})$ comes from the estimator in Section 5.2 and replaces $\boldsymbol{\Xi}_4^{-1}$ in (44). Note that the deduction of $\widehat{\boldsymbol{\mu}}_d$ consists of taking the time derivative of $\widehat{\boldsymbol{\xi}}_2$, producing $\dot{\widehat{\boldsymbol{\xi}}}_2 = \begin{bmatrix}\mathbf{0}_{3\times 7} & \mathbf{I}_3 & \mathbf{0}_{6\times 6}\end{bmatrix}\mathbf{P}_\zeta \mathbf{C}_\zeta^\top \mathbf{R}_\zeta^{-1}\widetilde{\mathbf{x}}$ in virtue of (9). For the construction of the estimator, $\widehat{T}$ and $\widehat{\boldsymbol{\tau}}$ are used to replace T and $\boldsymbol{\tau}$ in (46), which results in $\widehat{\mathbf{A}}_{\boldsymbol{\xi}}$. It is then used to replace $\mathbf{A}_{\boldsymbol{\xi}}$ in (8) that describes the estimator for $\boldsymbol{\xi}$. The estimator for $\boldsymbol{\eta}$ remains the same as that in Section (5.2). In the sequel, we present a diagram in Fig.

2 for the closed-loop interconnected system consisting of the plant, the controller, and the estimators, whose stability property is stated as follows.

Theorem 6.1. *Under Assumption 1, choose* $\boldsymbol{\delta}$ *such that* $\delta_3 \neq 0$. *Given a reference trajectory* $\mathbf{p}_d : \mathbb{R}_{\geq 0} \to \mathbb{R}^3$ *of at least class* $\mathcal{C}^3$ *with bounded time derivatives* $\dot{\mathbf{p}}_d$, $\ddot{\mathbf{p}}_d$, *and* $\dddot{\mathbf{p}}_d$, *consider the interconnected system consisting of the plant* (21) *driven by the control laws* (56) *and* (57) *and the estimator in Section 6. Suppose Assumption 2 holds with* T *and* $\boldsymbol{\tau}$ *replaced by* $\widehat{T}$ *and* $\widehat{\boldsymbol{\tau}}$, *then for every initial condition in* $\mathbb{R}^3 \times \mathsf{SO}(3) \times \mathbb{R}^6$, *there exists some sufficiently small initial estimation error such that the solution to* (21) *exists;* $\mathbf{v}$, $\boldsymbol{\omega}$, $\widehat{T}$, *and* $\widehat{\boldsymbol{\tau}}$ *are bounded on* $\mathbb{R}_{\geq 0}$; $t \mapsto \widehat{\mathbf{z}}(t)$ *is uniformly ultimately bounded by* $2\lambda_3^{-1}(\mathbf{K})\alpha\|\boldsymbol{\delta}\|$.

Proof. Please refer to Appendix D. □

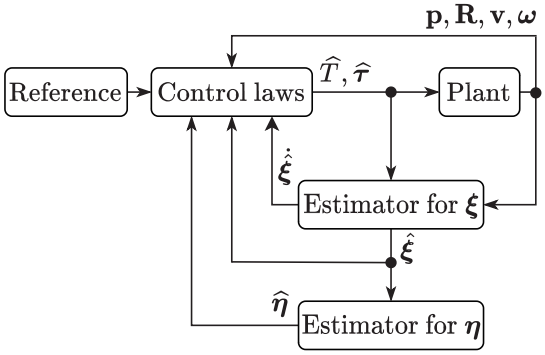

Figure 2. Diagram of the closed-loop system.

Remark 4. Notice that the conclusion in Theorem 6.1 holds locally, in the sense that the initial estimation error should be sufficiently small in order to guarantee a sufficiently large domain of attraction. In practice, however, convergence of the parameter estimator is independent from that of the backstepping errors. Then if the estimator is allowed to be turned on before the controller, there (so long as UCO is satisfied) exists some time after which the estimation errors are sufficiently small and ultimately boundedness can be achieved for any initial conditions. In other words, if there is a good initial estimate of the unknown parameters, then the initial estimates can be chosen such that ϵ_1 is arbitrarily small and hence the interconnected system will always stay within the region where (D8) is satisfied. Furthermore, one can turn on both the controller and the estimator at the same time, wait for the estimator to converge (so long as UCO is satisfied and no finite time escape occurs) so that there will be a time after which the interconnected system will stay within the region where (D8) is satisfied.

At this stage, we present the flowchart which illustrates the implementation procedures of our proposed control scheme, see Fig. 3, which serves as a guideline for subsequent simulations and experiments.

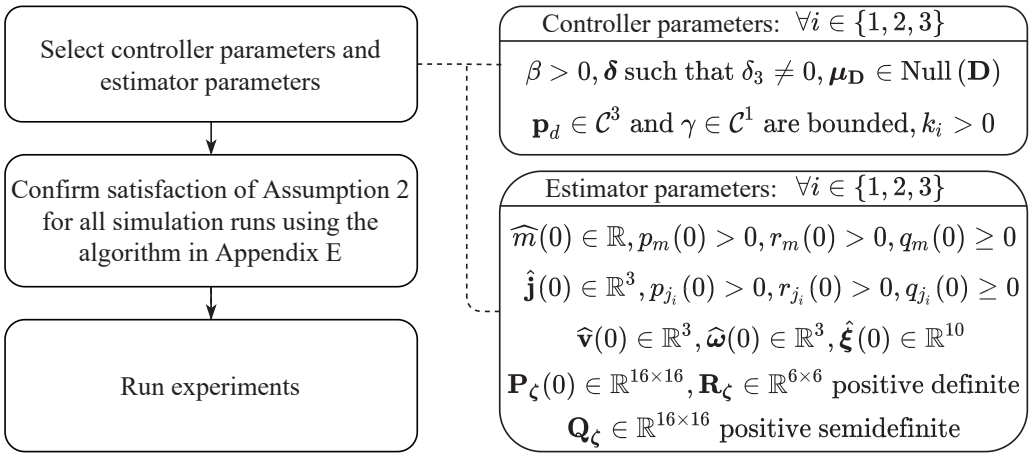

Figure 3. Implementation procedures of the proposed control scheme.

7. Simulation Results

In order to verify the performance of the proposed control laws, this section presents simulation results of the interconnected system consisting of the (21) driven by the control laws (56) and (57), the estimator for $\boldsymbol{\xi}$ in Section 5.1, and the estimator for $\boldsymbol{\eta}$ in Section 5.2, using MATLAB/Simulink. Through the following simulations, we attempt to highlight the importance of Assumption 2, the capability of robustness against Gaussian noises, and different levels of stability the controller and/or the estimator achieves.

The terminologies within subsequent subsection titles are interpreted in the following way: by *deterministic* we mean there is no random noise in the interconnected system; by *open-loop* we mean the parameter estimator is running in open-loop with the nominal controller as is the case in Section 5; by *stochastic*, we mean there is certain random noise in the interconnected system; by *closed-loop*, we mean the controller is fed with estimates coming from the parameter estimator as is the case in Section 6.

In Table 1, we summarize the parameters shared by all subsequent simulations. Moreover, unless redeclared, the following parameters are used by default. The initial values of the plant are: $\mathbf{p}(0) = [0\ 0\ 0]^\top$, $\mathbf{v}(0) = [0\ 0\ 0]^\top$, $\mathbf{R}(0) = \mathbf{I}_3$, $\boldsymbol{\omega}(0) = [0\ 0\ 0]^\top$. Initial values of the estimator are: $\widehat{\mathbf{v}}(0) = \mathbf{v}(0)$, $\widehat{\boldsymbol{\omega}}(0) = \boldsymbol{\omega}(0)$, $\widehat{\xi}_1(0) = 2\xi_1$, $\widehat{\boldsymbol{\xi}}_2(0) = -1.5\boldsymbol{\xi}_2, \widehat{\boldsymbol{\xi}}_3(0) = 0.5\boldsymbol{\xi}_3, \widehat{\boldsymbol{\xi}}_4(0) = 2\boldsymbol{\xi}_4, \mathbf{P}_{\boldsymbol{\zeta}}(0) = \text{diag}([10^{-3}\mathbf{1}_3^\top\ \mathbf{1}_3^\top\ 0.5\mathbf{1}_4^\top\ 50\mathbf{1}_3^\top\ 5{\cdot}10^5\mathbf{1}_3^\top]^\top)$, $\widehat{m}(0) = 0.5m$, $p_m(0) = q_m$, $\widehat{j}_1(0) = 0.5j_1$, $p_{j_1}(0) = q_{j_1}$, $\widehat{j}_2(0) = 0.5j_2$, $p_{j_2}(0) = q_{j_2}$, $\widehat{j}_3(0) = 0.5j_3$, $p_{j_3}(0) = q_{j_3}$.

7.1. Deterministic open-loop fixed-point tracking

In this simulation, we select the reference position $\mathbf{p}_d(t) = [0\ 0\ 0]^\top$ for every $t \in \mathbb{R}_{\geq 0}$, external disturbances $\mathbf{b} = [0\ 0\ 0]^\top$, the measurement noise covariance matrix $\mathbf{R}_{\boldsymbol{\zeta}} = 10^{-2}\mathbf{I}_6$, and the process noise covariance matrix $\mathbf{Q}_{\boldsymbol{\zeta}} = \text{diag}([10^{-3}\mathbf{1}_3^\top\ \mathbf{1}_3^\top\ 0.5\mathbf{1}_4^\top\ 50\mathbf{1}_3^\top\ 5{\cdot}10^5\mathbf{1}_3^\top]^\top)$.

We compare the estimator performance under different levels of "richness" of signals, which lead to satisfaction or violation of Assumption 2. To this end, we adopt the example in (49)-(52) that violates Assumption 2, namely the function γ in (36) to

Table 1. Parameters for the Simulation

Parameter	Value	Parameter	Value
m	0.2	r_m	1
$\mathbf{j}$	$10^{-3}[6\ 4\ 1]^\top$	q_m	1
g	9.8	r_{j_1}	10^4
k_1	2	q_{j_1}	10^{-2}
k_2	3	r_{j_2}	10^4
k_3	4	q_{j_2}	10^{-2}
β	2	r_{j_3}	10^4
$\boldsymbol{\mu}_\mathbf{D}$	$[0\ \boldsymbol{\delta}^\top]^\top$	q_{j_3}	10^{-2}

be $\gamma(t) = 0$ for every $t \in \mathbb{R}_{\geq 0}$ and $\boldsymbol{\delta} = [0\ 0\ 0.1]^\top$. After that, we generate "rich" signals by setting the function γ in (36) to be $\gamma(t) = 30 \sin t$ for every $t \in \mathbb{R}_{\geq 0}$ and $\boldsymbol{\delta} = [0.15\ \ -0.05\ 0.1]^\top$.

As seen in Fig. 4a, all of the estimation error norms remain constant after the initial transients. This is due to the fact that the signals are not "rich" enough to satisfy Assumption 2, which is rigorously analyzed for (49)-(52). Hence the failure in fulfillment of UCO can lead to a non-convergent estimator. On the contrary, all of the estimation error norms in Fig. 4a exponentially converge to zero, which is due to the fact that we are generating "richer" signals.

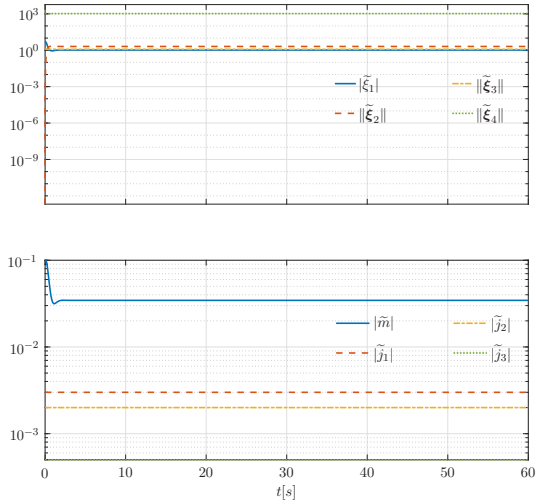

(a) Time evolution of the estimation error norms when $\gamma(t) = 0$ for every $t \in \mathbb{R}_{\geq 0}$ and $\boldsymbol{\delta} = [0\ 0\ 0.1]^\top$.

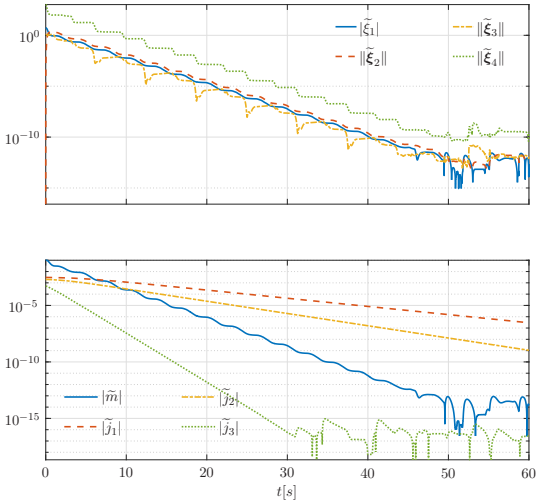

(b) Time evolution of the estimation error norms when $\gamma(t) = 30 \sin t$ for every $t \in \mathbb{R}_{\geq 0}$ and $\boldsymbol{\delta} = [0.15\ \ -0.05\ 0.1]^\top$.

Figure 4. Comparison between time evolutions of the estimation error norms for the deterministic open-loop fixed-point tracking under different levels of richness in signals (in log scale).

Since the nominal controller is running in open-loop with the estimator, the stability property in Lemma 4.2 holds and is independent from the choices of γ or $\boldsymbol{\delta}$, which is witnessed in Fig. 5. Note that in both cases, $\|\mathbf{z}_2\|$ and $\|\widehat{\mathbf{z}}_3\|$ approaches zero asymptotically. In Fig. 4a , $\|\mathbf{z}_1\|$ asymptotically converges to $0.05 = \frac{\delta_3}{k_1}$ as proved in

(49) when $k_1 \neq k_2$, and $\|\mathbf{z}_1\|$ remains within the theoretical bound $2k_1^{-1}\|\boldsymbol{\delta}\| = 0.1$ guaranteed in Lemma 4.2.

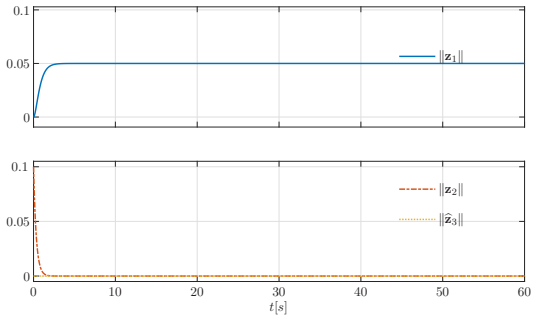

(a) Time evolution of the backstepping error norms when $\gamma(t) = 0$ for every $t \in \mathbb{R}_{\geq 0}$ and $\boldsymbol{\delta} = [0\ 0\ 0.1]^\top$.

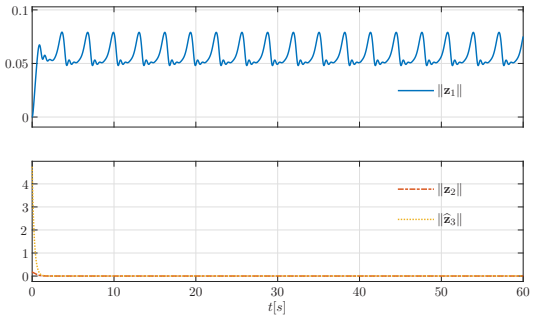

(b) Time evolution of the backstepping error norms when $\gamma(t) = 30\sin t$ for every $t \in \mathbb{R}_{\geq 0}$ and $\boldsymbol{\delta} = [0.15\ \ -0.05\ 0.1]^\top$.

Figure 5. Comparison between time evolutions of the backstepping error norms for the deterministic open-loop fixed-point tracking under different levels of richness in signals.

To check Assumption 2 for the simulation when $\gamma(t) = 0$ for every $t \in \mathbb{R}_{\geq 0}$ and $\boldsymbol{\delta} = [0\ 0\ 0.1]^\top$, we invoke the program presented in Appendix E, which returns no feasible $\Delta t > 0$ that satisfies the Assumption, no matter how small $\epsilon > 0$ may be. This is due to the fact that the specific choice $\mathbf{c}$ with $c_1 = 0$, $\mathbf{c}_2 = \mathbf{c}_4 = \mathbf{0}_{3\times 1}$ leads to violation of Assumption 2. This fact is rigorously analyzed for (49)-(52) and can also be extracted from the program by noticing that $\mathbf{c} \in \text{Null}\left(\int_t^\tau \mathbf{A}_{\boldsymbol{\zeta}}(\sigma)d\sigma\right)$ for any $t \geq t_0$ and $\tau \geq t$.

7.2. Stochastic open-loop fixed-point tracking

In this simulation, we select the reference position $\mathbf{p}_d(t) = [0\ 0\ 0]^\top$ for every $t \in \mathbb{R}_{\geq 0}$, external disturbances $\mathbf{b} = [0\ 0\ 0]^\top$, the function γ in (36) to be $\gamma(t) = 30\sin t$ for every $t \in \mathbb{R}_{\geq 0}$, and $\boldsymbol{\delta} = [0.15\ \ -0.05\ 0.1]^\top$. We add to the system (6) white Gaussian noises. Specifically, we consider open-loop estimation of the following plant dynamics corrupted by white Gaussian noises:

$$\begin{aligned}
\dot{\mathbf{p}}(t) &= \mathbf{R}(t)\mathbf{v}(t),\\
\dot{\mathbf{R}}(t) &= \mathbf{R}(t)\mathbf{S}(\boldsymbol{\omega}(t)),\\
\dot{\mathbf{v}}(t) &= -\mathbf{S}(\boldsymbol{\omega}(t))\mathbf{v}(t) + g\mathbf{R}^\top(t)\mathbf{e}_3 + m^{-1}\mathbf{R}^\top(t)\mathbf{b} - m^{-1}T(t)\mathbf{e}_3 + \mathbf{n}_{p,\mathbf{v}}(t),\\
\dot{\boldsymbol{\omega}}(t) &= -\mathbf{J}^{-1}\mathbf{S}(\boldsymbol{\omega}(t))\mathbf{J}\boldsymbol{\omega}(t) + \mathbf{J}^{-1}\boldsymbol{\tau}(t) + \mathbf{n}_{p,\boldsymbol{\omega}}(t),
\end{aligned} \tag{58}$$

where the process noise $\mathbf{n}_p(t) = [\mathbf{n}_{p,\mathbf{v}}^\top(t)\ \mathbf{n}_{p,\boldsymbol{\omega}}^\top(t)]^\top \in \mathbb{R}^6$ is zero-mean Gaussian processes with covariance $\mathbb{E}[\mathbf{n}_p(t)\mathbf{n}_p^\top(t)] = \text{diag}([10^{-3}\mathbf{1}_3^\top\ \mathbf{1}_3^\top]^\top)$. Similarly, the measured output is corrupted by white Gaussian noises:

$$\mathbf{y}(t) = \begin{bmatrix} \mathbf{v}(t) + \mathbf{n}_{m,\mathbf{v}}(t) \\ \boldsymbol{\omega}(t) + \mathbf{n}_{m,\boldsymbol{\omega}}(t), \end{bmatrix} \tag{59}$$

where the measurement noise $\mathbf{n}_m(t) = [\mathbf{n}_{m,\mathbf{v}}^\top(t)\ \mathbf{n}_{m,\boldsymbol{\omega}}^\top(t)]^\top \in \mathbb{R}^6$ is zero-mean Gaussian processes with covariance $\mathbb{E}[\mathbf{n}_m(t)\mathbf{n}_m^\top(t)] = 10^{-2}\mathbf{I}_6$. Note that the process noise $\mathbf{n}_p(t)$

and the measurement noise $\mathbf{n}_m(t)$ are chosen to be uncorrelated.

We compare the estimator performance under different noise covariance matrices. The estimator performance is evaluated based on the signal-to-noise ratio defined as

$$\text{SNR} = \left\| \mathbf{P}_{\boldsymbol{\zeta}} \mathbf{C}_{\boldsymbol{\zeta}}^{\top} \mathbf{R}_{\boldsymbol{\zeta}}^{-1} \right\|, \tag{60}$$

which is essentially the maximum singular value of the gain $\mathbf{K}_{\boldsymbol{\zeta}}$ in (8), see (Maybeck, 1979, Chapter 5.11) for details. For sake of simplicity in presentation, we define $\overline{\mathbf{R}}_{\boldsymbol{\zeta}} = 10^{-2}\mathbf{I}_6$ as the baseline measurement noise covariance matrix and $\overline{\mathbf{Q}}_{\boldsymbol{\zeta}} = \text{diag}([10^{-3}\mathbf{1}_3^{\top}\ \mathbf{1}_3^{\top}\ 0.5\mathbf{1}_4^{\top}\ 50\mathbf{1}_3^{\top}\ 5\cdot 10^5\mathbf{1}_3^{\top}]^{\top})$ as the baseline process noise covariance matrix.

In Table 2, the mean values of the SNR in steady state for different combinations of the covariance matrices are presented. Under the same $\mathbf{Q}_{\boldsymbol{\zeta}}$, a smaller $\mathbf{R}_{\boldsymbol{\zeta}}$ leads to a larger mean SNR. Under the same $\mathbf{R}_{\boldsymbol{\zeta}}$, a larger $\mathbf{Q}_{\boldsymbol{\zeta}}$ leads to a larger mean SNR. These phenomena meet our expectation in the sense that the noises will be greater attenuated if we have more trust about the certainty of the measurement.

Table 2. Attenuation of noises in steady state under different covariance matrices

$\mathbf{R}_{\boldsymbol{\zeta}}$	$0.01\overline{\mathbf{R}}_{\boldsymbol{\zeta}}$	$0.1\overline{\mathbf{R}}_{\boldsymbol{\zeta}}$	$0.1\overline{\mathbf{R}}_{\boldsymbol{\zeta}}$	$\overline{\mathbf{R}}_{\boldsymbol{\zeta}}$	$10\overline{\mathbf{R}}_{\boldsymbol{\zeta}}$	$10\overline{\mathbf{R}}_{\boldsymbol{\zeta}}$	$100\overline{\mathbf{R}}_{\boldsymbol{\zeta}}$
$\mathbf{Q}_{\boldsymbol{\zeta}}$	$0.1\overline{\mathbf{Q}}_{\boldsymbol{\zeta}}$	$0.1\overline{\mathbf{Q}}_{\boldsymbol{\zeta}}$	$\overline{\mathbf{Q}}_{\boldsymbol{\zeta}}$	$\overline{\mathbf{Q}}_{\boldsymbol{\zeta}}$	$\overline{\mathbf{Q}}_{\boldsymbol{\zeta}}$	$10\overline{\mathbf{Q}}_{\boldsymbol{\zeta}}$	$10\overline{\mathbf{Q}}_{\boldsymbol{\zeta}}$
mean SNR($\cdot 10^3$)	30.43	7.47	29.00	9.27	2.91	9.24	2.89

To check Assumption 2 for this simulation, we invoke the program presented in Appendix E, recursively on the lower limit of the integral (48), namely $t \in \{0, 0.1, 0.2, \ldots, 50\}$. The program return $\Delta t = 1.55$ and $\epsilon = 0.001$ that satisfy the Assumption.

We remark here that though the notion of UCO in this paper is introduced for deterministic settings, the very same definition here is used for stochastic settings as well, see (Kamen & Su, 1999, Chapter 6.3). The same remark works for Section 7.4. Therefore, we are allowed to check Assumption 2 without worrying the stochastic nature of these simulations.

7.3. Deterministic closed-loop fixed-point tracking

In this simulation, we select the reference position $\mathbf{p}_d(t) = [0\ 0\ 0]^{\top}$ for every $t \in \mathbb{R}_{\geq 0}$, external disturbances $\mathbf{b} = [0\ 0\ 0]^{\top}$, the function γ in (36) to be $\gamma(t) = 30\sin t$ for every $t \in \mathbb{R}_{\geq 0}$, and $\boldsymbol{\delta} = [0.15\ \ -0.05\ 0.1]^{\top}$. For sake of simplicity in presentation, we define $\overline{\mathbf{R}}_{\boldsymbol{\zeta}} = 10^{-2}\mathbf{I}_6$ as the baseline measurement noise covariance matrix and $\overline{\mathbf{Q}}_{\boldsymbol{\zeta}} = \text{diag}([10^{-3}\mathbf{1}_3^{\top}\ \mathbf{1}_3^{\top}\ 0.5\mathbf{1}_4^{\top}\ 50\mathbf{1}_3^{\top}\ 5\cdot 10^5\mathbf{1}_3^{\top}]^{\top})$ as the baseline process noise covariance matrix.

Under different combinations of $\mathbf{R}_{\boldsymbol{\zeta}}$ and $\mathbf{Q}_{\boldsymbol{\zeta}}$, we compare convergence rates of the estimates by presenting the decay of the associated Lyapunov functions $V_1^e : \mathbb{R}_{\geq 0} \times \mathbb{R}^{16} \to \mathbb{R}$ and $V_2^e : \mathbb{R}_{\geq 0} \times \mathbb{R}^4 \to \mathbb{R}$ defined by

$$V_1^e(t, \widetilde{\boldsymbol{\zeta}}) = \widetilde{\boldsymbol{\zeta}}^{\top} \mathbf{P}_{\boldsymbol{\zeta}}^{-1}(t) \widetilde{\boldsymbol{\zeta}} \tag{61}$$

for the parameter estimator for $\boldsymbol{\xi}$, and

$$V_2^e(t, \widetilde{\boldsymbol{\eta}}) = p_m^{-1}(t)\widetilde{m}^2 + \sum_{i=1}^{3} p_{j_i}^{-1}(t)\widetilde{j}_i^2 \tag{62}$$

for the parameter estimator for $\boldsymbol{\eta}$.

As witnessed in Fig. 6a and Fig. 6b, a smaller $\mathbf{R}_{\boldsymbol{\zeta}}$ implies faster convergence rate of the Lyapunov function V_1^e, while a larger $\mathbf{Q}_{\boldsymbol{\zeta}}$ implies faster convergence rate of the Lyapunov function V_1^e. However, this relationship is not that clear for the convergence rate of the Lyapunov function V_2^e. These phenomena can be analyzed by considering the time derivative of the Lyapunov functions, namely:

$$\dot{V}_1^e(t, \widetilde{\boldsymbol{\zeta}}) = -\widetilde{\boldsymbol{\zeta}}^\top (\mathbf{P}_{\boldsymbol{\zeta}}^{-1}(t)\mathbf{Q}_{\boldsymbol{\zeta}}\mathbf{P}_{\boldsymbol{\zeta}}(t) + \mathbf{C}_{\boldsymbol{\zeta}}^\top \mathbf{R}_{\boldsymbol{\zeta}}^{-1}\mathbf{C}_{\boldsymbol{\zeta}})\widetilde{\boldsymbol{\zeta}}, \tag{63}$$

hence a smaller $\mathbf{R}_{\boldsymbol{\zeta}}$ or a larger $\mathbf{Q}_{\boldsymbol{\zeta}}$ can speed up the convergence; and

$$\begin{aligned}\dot{V}_2^e(t, \widetilde{\boldsymbol{\eta}}) = &- \widetilde{m}^2(p_m^{-2}(t)q_m + \widehat{\xi}_1^2(t)r_m^{-1}) - 2r_m^{-1}\widehat{\xi}_1(t)\widetilde{\xi}_1(t)m\widetilde{m} \\ &- \sum_{i=1}^{3}\left(\widetilde{j}_i^2(p_{j_i}^{-2}(t)q_{j_i} + (\mathbf{e}_i^\top \widehat{\boldsymbol{\xi}}_4(t))^2 r_{j_i}^{-1}) + 2r_{j_i}^{-1}(\mathbf{e}_i^\top \widehat{\boldsymbol{\xi}}_4(t))(\mathbf{e}_i^\top \widetilde{\boldsymbol{\xi}}_4(t))j_i\widetilde{j}_i\right),\end{aligned} \tag{64}$$

hence $\dot{V}_2^e$ is dominated by the second order term when $\widetilde{\boldsymbol{\eta}}$ is large, but is dominated by the first order term when it becomes smaller. Therefore, the convergence rates of V_2^e are indistinguishable during the initial transients, but is more affected afterwards.

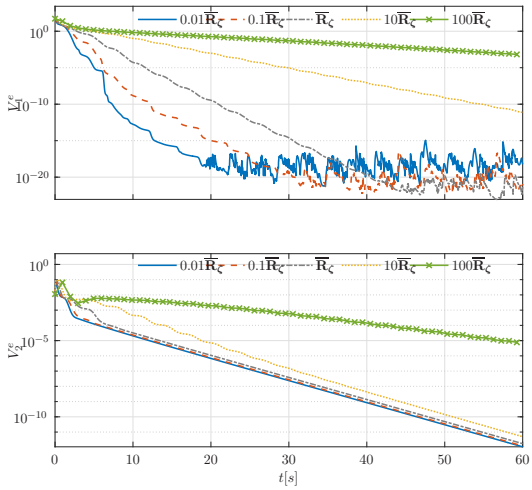

(a) Time evolutions of V_1^e and V_2^e in (61) and (62) under different $\mathbf{R}_{\boldsymbol{\zeta}}$ with fixed $\mathbf{Q}_{\boldsymbol{\zeta}} = \overline{\mathbf{Q}}_{\boldsymbol{\zeta}}$.

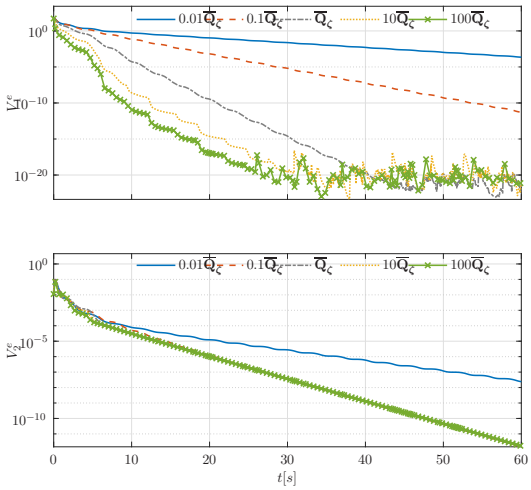

(b) Time evolutions of V_1^e and V_2^e in (61) and (62) under different $\mathbf{Q}_{\boldsymbol{\zeta}}$ with fixed $\mathbf{R}_{\boldsymbol{\zeta}} = \overline{\mathbf{R}}_{\boldsymbol{\zeta}}$.

Figure 6. Comparison between time evolutions of the Lyapunov functions V_1^e and V_2^e in (61) and (62) for the deterministic closed-loop fixed-point tracking under different noise covariance matrices (in log scale).

It is also interesting to see the time evolution of the backstepping error norm $\|\mathbf{z}_1\|$ for the simulations above. A smaller $\mathbf{R}_{\boldsymbol{\zeta}}$ or a larger $\mathbf{Q}_{\boldsymbol{\zeta}}$ contributes to shorter transients of the backstepping error norm $\|\mathbf{z}_1\|$, which is due to a faster parameter adaption as shown above. Despite initial errors, $\mathbf{z}_1$ stays within a ball around zero of radius

about 0.08 m after the initial transient for about 5 seconds. It is clear that the steady state error of is smaller than the theoretical infimum of the ultimate bound, namely $\inf_{\theta_3 \in (0,1)} \theta_3^{-1} \lambda_3^{-1}(\mathbf{K}) \alpha \|\boldsymbol{\delta}\| = 1.596$, that appears in the proof of Theorem 6.1.

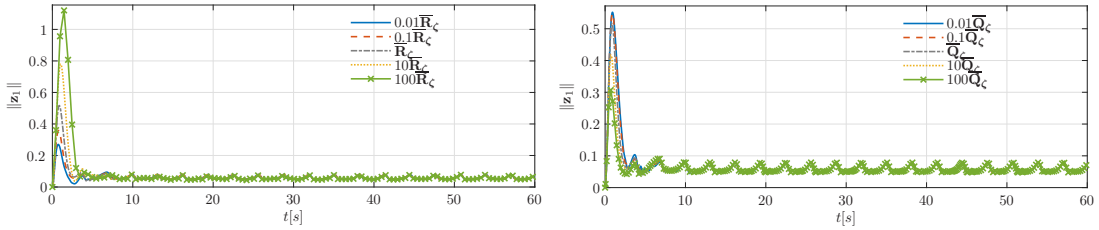

(a) Time evolution of the backstepping error norm $\|\mathbf{z}_1\|$ under different $\mathbf{R}_\zeta$ with fixed $\mathbf{Q}_\zeta = \overline{\mathbf{Q}}_\zeta$.

(b) Time evolution of the backstepping error norm $\|\mathbf{z}_1\|$ under different $\mathbf{Q}_\zeta$ with fixed $\mathbf{R}_\zeta = \overline{\mathbf{R}}_\zeta$.

Figure 7. Comparison between time evolutions of the backstepping error norm $\|\mathbf{z}_1\|$ for the deterministic closed-loop fixed-point tracking under different noise covariance matrices.

To check Assumption 2 for this simulation, we invoke the program presented in Appendix E, recursively on the lower limit of the integral (48), namely $t \in \{0, 0.1, 0.2, \ldots, 50\}$. The program return $\Delta t = 1.65$ and $\epsilon = 0.001$ that satisfy the Assumption.

7.4. Stochastic closed-loop lemniscate tracking

In this simulation, we select the function γ in (36) to be $\gamma(t) = 30 \sin t$ for every $t \in \mathbb{R}_{\geq 0}$, $\boldsymbol{\delta} = [0.15 \ -0.05 \ 0.1]^\top$, the external disturbances $\mathbf{b} = [-0.3 \ 0.2 \ -0.1]^\top$. The reference trajectory is a tilted lemniscate defined as

$$\mathbf{p}_d(t) = \mathbf{R}_x(\phi) \begin{bmatrix} \dfrac{\ell_d \sin\psi(t) \cos\psi(t)}{(\cos\psi(t))^2 + 1} \\ \dfrac{\ell_d \sin\psi(t)}{(\sin\psi(t))^2 + 1} \\ -\ell_d \end{bmatrix} \tag{65}$$

for every $t \in \mathbb{R}_{\geq 0}$, where

$$\dot{\psi}(t) = \frac{v_d(t)}{\ell_d} \sqrt{\sin^2(t) + 1} \tag{66}$$

with $v_d(t) \in \mathbb{R}_{\geq 0}$ defining the desired linear speed at each instant, and

$$\mathbf{R}_x(\phi) = \begin{bmatrix} 1 & 0 & 0 \\ 0 & \cos(\phi) & \sin(\phi) \\ 0 & -\sin(\phi) & \cos(\phi) \end{bmatrix}. \tag{67}$$

We set $\phi = -10°$, $\ell_d = 1.2$, and $v_d(t) = 0.8$ for every $t \in \mathbb{R}_{\geq 0}$. We add to the system (6) white Gaussian noises. Specifically, we consider open-loop estimation of the following

plant dynamics corrupted by white Gaussian noises:

$$\begin{aligned}
\dot{\mathbf{p}}(t) &= \mathbf{R}(t)\mathbf{v}(t),\\
\dot{\mathbf{R}}(t) &= \mathbf{R}(t)\mathbf{S}(\boldsymbol{\omega}(t)),\\
\dot{\mathbf{v}}(t) &= -\mathbf{S}(\boldsymbol{\omega}(t))\mathbf{v}(t) + g\mathbf{R}^\top(t)\mathbf{e}_3 + \mathbf{R}(t)^\top\boldsymbol{\xi}_2(t) - \xi_1(t)T(t)\mathbf{e}_3 + \mathbf{n}_{p,\mathbf{v}}(t),\\
\dot{\boldsymbol{\omega}}(t) &= \boldsymbol{\Omega}(\boldsymbol{\omega}(t))\boldsymbol{\xi}_3(t) + \mathbf{U}(\boldsymbol{\tau}(t))\boldsymbol{\xi}_4(t) + \mathbf{n}_{p,\boldsymbol{\omega}}(t),\\
\dot{\boldsymbol{\xi}}(t) &= \mathbf{n}_{p,\boldsymbol{\xi}}(t),
\end{aligned} \tag{68}$$

where the process noise $\mathbf{n}_p(t) = [\mathbf{n}_{p,\mathbf{v}}^\top(t)\ \mathbf{n}_{p,\boldsymbol{\omega}}^\top(t)\ \mathbf{n}_{p,\boldsymbol{\xi}}^\top(t)]^\top \in \mathbb{R}^{16}$ is zero-mean Gaussian processes with covariance $\mathbb{E}[\mathbf{n}_p(t)\mathbf{n}_p^\top(t)] = n_p\mathbf{I}_{16}$. Similarly, the measured output is corrupted by white Gaussian noises:

$$\mathbf{y}(t) = \begin{bmatrix}\mathbf{v}(t) + \mathbf{n}_{m,\mathbf{v}}(t)\\ \boldsymbol{\omega}(t) + \mathbf{n}_{m,\boldsymbol{\omega}}(t),\end{bmatrix} \tag{69}$$

where the measurement noise $\mathbf{n}_m(t) = [\mathbf{n}_{m,\mathbf{v}}^\top(t)\ \mathbf{n}_{m,\boldsymbol{\omega}}^\top(t)]^\top \in \mathbb{R}^6$ is zero-mean Gaussian processes with covariance $\mathbb{E}[\mathbf{n}_m(t)\mathbf{n}_m^\top(t)] = 10^{-2}\mathbf{I}_6$. Note that the process noise $\mathbf{n}_p(t)$ and the measurement noise $\mathbf{n}_m(t)$ are chosen to be uncorrelated. Moreover, we select the measurement noise covariance matrix $\mathbf{R}_{\boldsymbol{\zeta}} = 10^{-2}\mathbf{I}_6$ and the process noise covariance matrix $\mathbf{Q}_{\boldsymbol{\zeta}} = \mathrm{diag}([10\mathbf{1}_{13}^\top\ 10^3\mathbf{1}_3^\top]^\top)$. This represents the practical case where one is often quite certain about the statistics of the measurement noise but uncertain about the statistics of the process noise. We select $\mathbf{P}_{\boldsymbol{\zeta}}(0) = \mathbf{Q}_{\boldsymbol{\zeta}}$.

We compare time evolutions of the backstepping error $\|\mathbf{z}_1\|$ under different process noises whose magnitudes are controlled by n_p. As witnessed in Fig. 8a, with a larger magnitude of the process noise, the steady-state backstepping error tends to increase. However, the transients performance under different n_p is nearly indistinguishable. This is due to the fact that we are fixing $\mathbf{P}_{\boldsymbol{\zeta}}(0)$, $\mathbf{R}_{\boldsymbol{\zeta}}$, and $\mathbf{Q}_{\boldsymbol{\zeta}}$, hence the convergence rates are nearly the same in view of (63) and consequently the time evolutions during the transients are nearly the same. For different n_p, the resulting mean signal-to-noise ratio in steady-state turns out to be around 400, see (60). We remark here the stability or boundedness of the backstepping errors is not analyzed for the stochastic setting. The purpose of this simulation is to show practical feasibility of our method and provide a foundation for further experimental verification.

Regarding the parameter estimator performance, we present the time evolutions of V_1^e in (61) under different process noises whose magnitudes are controlled by n_p. As witnessed in Fig. 8b, with a smaller magnitude of the process noise, the Lyapunov function tends to decrease further to zero. It can be theoretically proved that, in the stochastic setting like in the case here, the parameter estimator is asymptotically unbiased, see (Kamen & Su, 1999, Theorem 6.2). Hence the Lyapunov function should have been approaching to zero as time goes to infinity. However, this is not the situation presented in Fig. 8b as V_1^e stops decreasing and begins oscillating, which is especially obvious when $n_p = 100$. This phenomenon may comes from the fact that the noises we generate in simulations are not exactly uncorrelated white Gaussian processes.

To check Assumption 2 for this simulation, we invoke the program presented in Appendix E, recursively on the lower limit of the integral (48), namely $t \in \{0, 0.1, 0.2, \ldots, 50\}$. The program return $\Delta t = 1.05$ and $\epsilon = 0.001$ that satisfy the Assumption.

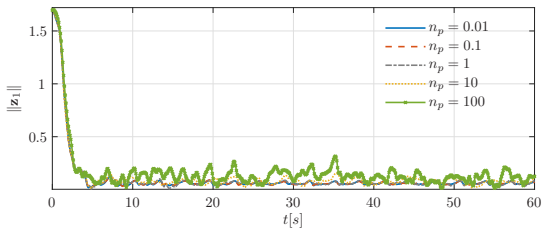

(a) Time evolutions of the backstepping error $\|\mathbf{z}_1\|$ under different process noises $\mathbb{E}[\mathbf{n}_p(t)\mathbf{n}_p^\top(t)] = n_p\mathbf{I}_{16}$ by varying n_p.

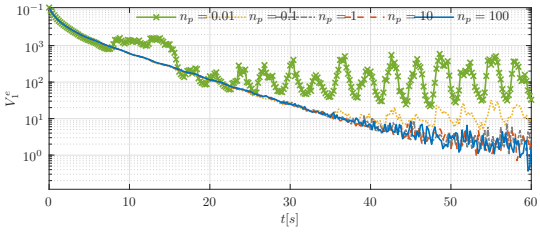

(b) Time evolutions of the Lyapunov function V_1^e in (61) under different process noises $\mathbb{E}[\mathbf{n}_p(t)\mathbf{n}_p^\top(t)] = n_p\mathbf{I}_{16}$ by varying n_p (in log scale).

Figure 8. Comparison between time evolutions of the backstepping error norm $\|\mathbf{z}_1\|$ and those of the Lyapunov function V_1^e in (61) for the stochastic closed-loop lemniscate tracking under process noises of different magnitudes.

8. Experimental Setup

Once the overall closed loop system including the interconnected system of the proposed parameter estimator and controller has been simulated and its performance assessed, the rapid prototyping and testing setup at the SCORE laboratory Sensor based Cooperative Robotics Research (SCORE) laboratory, at the Department of Electrical and Computer Engineering of the Faculty of Science and Technology, University of Macau. `http://score.fst.umac.mo/` (2018), University of Macau, was used to experimentally validate our algorithm. Experiments were conducted in a MATLAB/Simulink environment that integrated an optical motion capture system Vicon Motion Systems Ltd. `https://www.vicon.com/` (2018), and radio communication with the quadcopter. The quadcopter used for the experiments is a radio controlled BLADE 200QX. The vehicle has a flying weight of 0.217 kg (batteries, radio receiver, and motion capture markers included) and an inertia matrix of $10^{-4}\text{diag}([6.5\ 6.5\ 13])\,\text{kg}\,\text{m}^2$. It has four brushless motors which drive four propellers located at the end of each arm.

The experimental quadcopter lacks on-board sensors and the state of the quadcopter must be estimated resorting to external sensors. To this end, we placed six motion capture markers on the quadcopter. Meanwhile, the indoor motion capture system VICON is able to locate and measure the positions of the markers accurately, from which the position and orientation of the vehicle are obtained. VICON is a high performance system that is able to operate with sub-millimeter accuracy at up to 120 Hz. The performance of VICON is such that the linear velocity can be well estimated from the position measurements by a simple backwards Euler difference, with relatively low noise level. These measurements are then used to compute command signals, namely thrust and angular velocity, that control the motion of the quadcopter.

A graphical representation of the overall architecture is shown in Fig. 9. We used three computer systems, one running the Vicon motion tracking software; a second one consisted of the controller and the estimator which generates the command signals to be sent to the third computer through Ethernet; the third one receives the command signals and sends them through serial port to the RF module at time intervals of 45 ms. This is mainly to avoid jitter in the transmission of the serial port signals to the RF module when running all the systems in the same computer which can lead to erratic communication with the quadcopter.

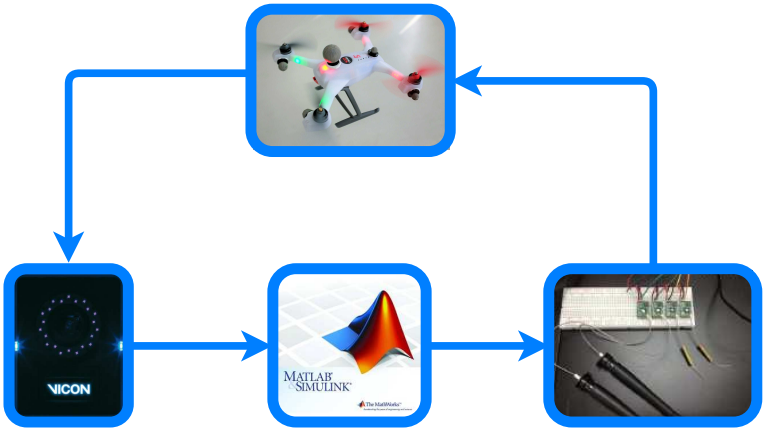

Figure 9. Quadcopter integrated measurement and command architecture.

9. Experimental Results

We performed two types of experiments in order to test the performance of the proposed controller. The first type has the same control task as in Section 7 to track a lemniscate trajectory. The second type aims to test adaptivity of the controller during hovering by adding extra weight to the quadcopter.

9.1. Tracking of a lemniscate trajectory

The lemniscate remains the same as that of Section 7. Figure 10 displays the reference trajectory and the actual position of the quadcopter, in which we can see that the vehicle is able to track the reference trajectory closely despite the initial position error. Time evolution of each backstepping error is shown in Fig. 11. Besides the decreasing tendency of the position error, both velocity errors are witnessed to decease in norm and then stay within some neighborhood around zero. The calculated root mean square of $\|\mathbf{z}_1\|$, $\|\mathbf{z}_2\|$, and $\|\widehat{\mathbf{z}}_3\|$ in steady state are 0.06 m, 0.21 m s^{-1}, and 6.95 s^{-1}, respectively. Reasons for these relative large (compared to the theoretical ultimate bound) steady state errors are manifold. On one hand, there are unmodeled dynamics of the quadcopter model, e.g., inner control loop that is assumed to operate sufficiently fast. On the other hand, the command signal sent to the quadcopter is obtained using the integral of the computed torque along time.

Figures 12a, 12b, 12c, and 12d show the performance of the estimator for $\boldsymbol{\xi}$. The estimate errors $|\widetilde{\xi}_1|$, $\|\widetilde{\boldsymbol{\xi}}_3\|$, and $\|\widetilde{\boldsymbol{\xi}}_4\|$ tend to zero as time increases. Since we do not have direct measure of $\boldsymbol{\xi}_2$, $\|\widehat{\boldsymbol{\xi}}_2\|$ gives an estimate for the external force disturbances with a magnitude of roughly 0.06 N. The oscillation pattern of $\|\widehat{\boldsymbol{\xi}}_2\|$ could be highly correlated with our choice of reference trajectory, which is periodic in time with period 2π. Figures 13a and 13b show the performance of the estimator for $\boldsymbol{\eta}$. It is clear that $\widehat{m}$ and $\widehat{\mathbf{j}}$ approach their actual values as time increases.

Actuation signals $\widehat{T}$ and $\widehat{\boldsymbol{\tau}}$ are shown in Fig. 14, in which there is a surge for both signal during the initial transients due to of the estimated parameters.

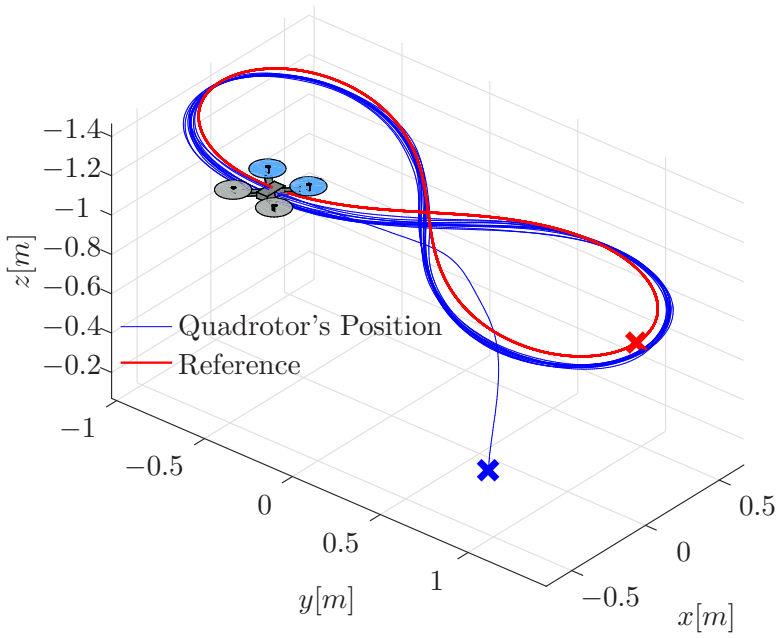

Figure 10. Three dimensional plot of the experimental result of the quadcopter position versus the lemniscate reference trajectory.

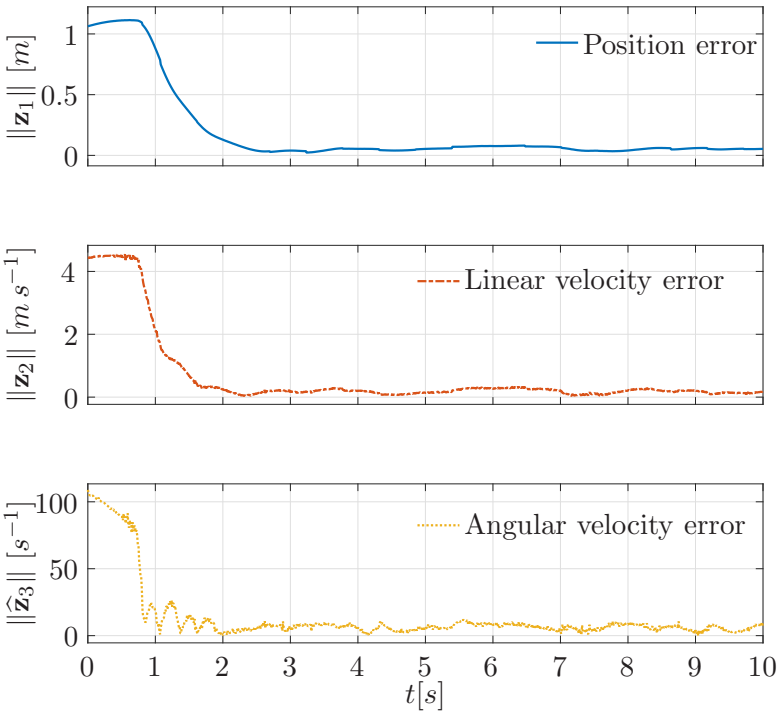

Figure 11. Time evolution of backstepping error norms.

9.2. Adding weight while hovering

The hovering point is chosen as $\mathbf{p}_d(t) = [0\ 0\ -0.8]$. While the quadcopter stayed closely to the fixed point, we attached an extra weight of 0.045 kg on top at around 35.2 seconds. This instant is marked with a gray line in subsequent figures.

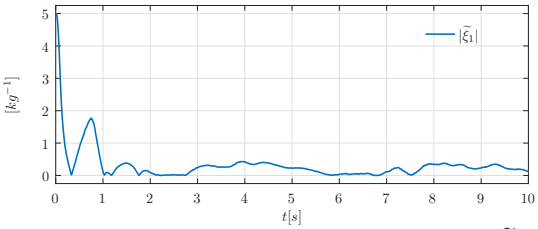

(a) Time evolution of the estimation error norm $|\widetilde{\xi}_1|$.

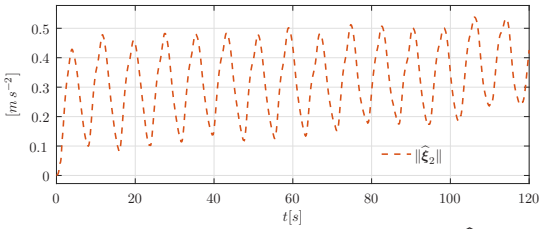

(b) Time evolution of the estimate norm $\|\widehat{\boldsymbol{\xi}}_2\|$.

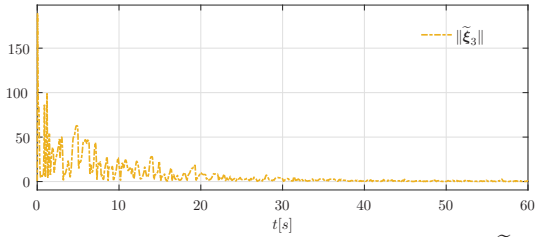

(c) Time evolution of the estimation error norm $\|\widetilde{\boldsymbol{\xi}}_3\|$.

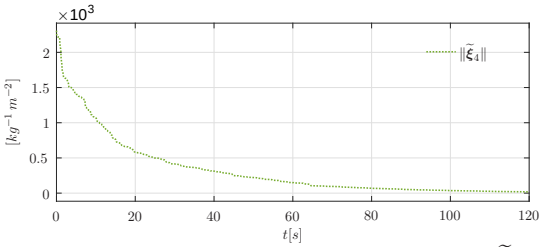

(d) Time evolution of the estimation error norm $\|\widetilde{\boldsymbol{\xi}}_4\|$.

Figure 12. Performance of the estimator for $\boldsymbol{\xi}$.

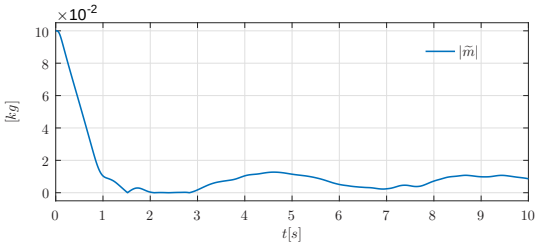

(a) Time evolution of the estimation error norm $|\widetilde{m}|$.

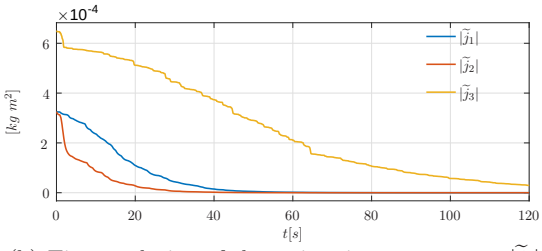

(b) Time evolution of the estimation error norms $|\widetilde{j}_i|$ with $i \in \{1, 2, 3\}$.

Figure 13. Performance of the estimator for $\boldsymbol{\eta}$.

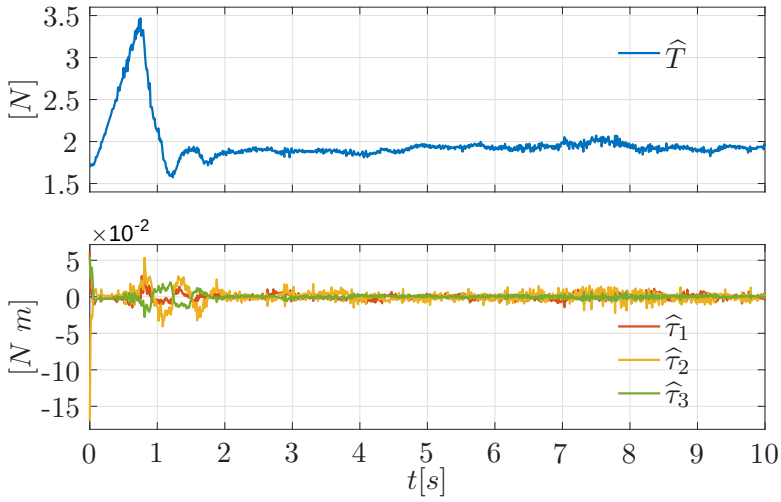

Figure 14. Time evolution of the actuation signals.

It can be seen from Fig. 15 that the position error suffers an increase in magnitude (around 0.05 m) when the extra weight is attached, but soon decreases and stays therein. The velocity errors are less influenced by this extra weight and are therefore not presented. Before adding the extra weight, the calculated root mean square of $\|\mathbf{z}_1\|$, $\|\mathbf{z}_2\|$, and $\|\widehat{\mathbf{z}}_3\|$ in steady state are 0.04 m, 0.18 m s^{-1}, and 6.60 s^{-1}, respectively. After adding the extra weight, their root mean square are 0.04 m, 0.18 m s^{-1}, and 6.55 s^{-1}, respectively.

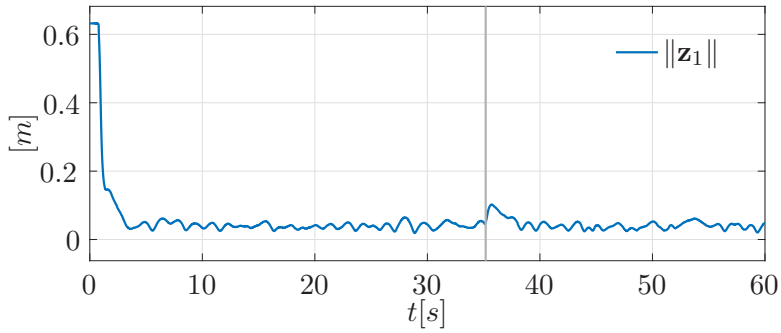

Figure 15. Time evolution of position error norm.

Comparing to other estimates, $\widehat{\xi}_1$ and $\widehat{m}$ undergoes more obvious change when the extra weight is added, as seen in Fig. 16 and Fig. 17. Before and after adding the extra weight, the amount of change in $\widehat{\xi}_1$ corresponds to a mass change of around $\frac{1}{4.35} - \frac{1}{5.32} \approx 0.042\,\text{kg}$ while the change in $\widehat{m}$ is around $0.231 - 0.188 \approx 0.043\,\text{kg}$. Both quantities reflect the adaptive feature of the proposed controller that reacts against the extra weight of 0.045 kg.

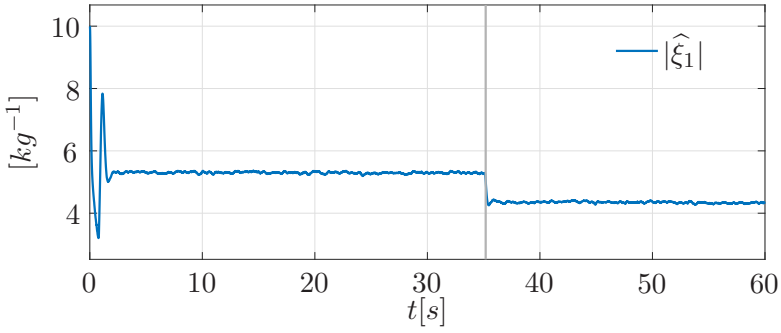

Figure 16. Time evolution of the estimate $\widehat{\xi}_1$.

The thrust force signal is shown in Fig. 18, in which it increases in magnitude to bear the extra weight.

For comparison, a separate experiment was done with a controller using static mass and inertia parameters, proposed in Xie, Yu, Cabecinhas, Cunha, and Silvestre (2021). Both the hovering point and the mass of the extra weight keep unchanged, resulting in the time evolution of the position error norm presented in Fig. 19. It is clear that the position error increases in magnitude when the extra weight is attached at around 23.5 seconds and goes from the old steady state with a calculated root mean square of 0.05 m to a new steady state with a calculated root mean square of 0.11 m. This demonstrates the effectiveness of the parameter estimator proposed in this paper, which contributes to adaptivity of our controller.

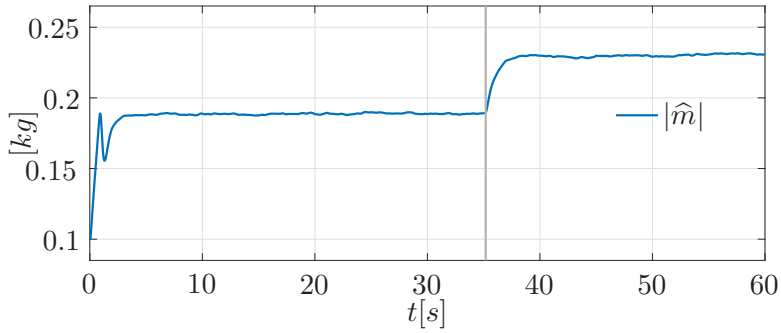

Figure 17. Time evolution of the estimate $\widehat{m}$.

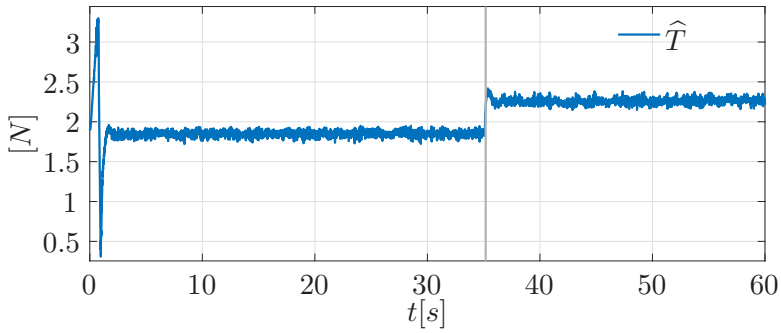

Figure 18. Time evolution of the thrust force.

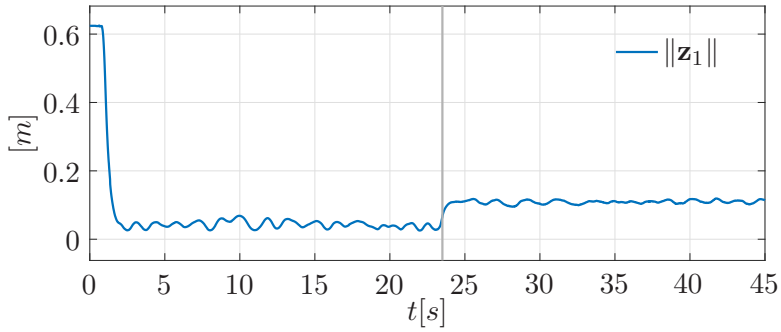

Figure 19. Time evolution of position error norm.

10. Conclusion

This paper presented a solution to the problem of trajectory tracking for quadcopter subject to parametric uncertainties and disturbances. A Kalman-Bucy filter based parameter estimator is designed on top of a backstepping controller to recover the unknown parameters, including the mass, the external force disturbances, and the moment of inertia. Under certain observability condition, we prove exponential stability of the estimator and uniform ultimate boundedness of the interconnected system consisting of the plant, the parameter estimator, and the backstepping controller. Through extensive simulations and experiments, we verified: (a) exponential stability of the open-loop parameter estimator in deterministic setting; (b) global practical stability of the open-loop nominal controller in deterministic setting; (c) practical stability of the interconnected system in deterministic setting; (d) asymptotic unbiased property and robustness of the open-loop/closed-loop parameter estimator in stochas-

tic setting; (e) adjustment of the estimation convergence rate through tuning the noise covariance matrices; (f) the versatility and usefulness of the program we developed to check the uniform complete observability condition; (g) robustness of the proposed control scheme against added mass that results in payload change in flight tasks. The future works extending the results in this paper are the following: studying a generic matrix rather than a diagonal one that represents the moment of inertia; investigating the role of γ in satisfaction or violation of the uniform complete observability condition; deriving conditions for stability of the interconnected system in stochastic settings; designing control laws for regulation of the yaw dynamics.

Data Availability Statement

The data that support the findings of this study are available from the authors, ZHU Xuan-Zhi and Wei Xie, upon reasonable request.

Funding

This work was supported in part by the Macao Science and Technology Development Fund under Grant FDCT/0031/2020/AFJ, in part by the University of Macau, Macao, China, under Project MYRG2018- 00198-FST, in part by the Fundao para a Cincia e a Tecnologia (FCT) through LARSyS - FCT Project UIDB/50009/2020 and LAETA - FCT Project UIDB/50022/2020, and by FCT project DECENTER [LISBOA-01-0145-FEDER-029605], in part by the Programa Operacional Regional de Lisboa 2020 and PIDDAC programs, and in part by FCT Scientific Employment Stimulus grants CEECIND/04199/2017 and CEECIND/04652/2017.

Disclosure statement

No potential conflict of interest was reported by the author(s).

Notes on contributor(s)

Xuan-Zhi Zhu, received the B.S. degree in Electrical and Computer Engineering from the University of Macau, Macau, China, in 2017. He is currently pursuing a Ph.D. degree at the Instituto Superior Tcnico, Universidade de Lisboa, Lisbon, Portugal. His research interests include sampled-data control, event-triggered control, and hybrid dynamical systems.

David Cabecinhas, received the Licenciatura and Ph.D. degrees in electrical and computer engineering from the Instituto Superior Tcnico, Universidade de Lisboa, Lisbon, Portugal, in 2006 and 2014, respectively. He is currently a Researcher with the Laboratory for Robotics and Engineering Systems, Institute for Systems and Robotics, Lisbon. His current research interests include nonlinear control, sensor-based and vision-based control, modeling and identification, and fault detection and mitigation with applications to autonomous aerial, surface, and underwater robotic vehicles.

Wei Xie, received the M.Sc. degree in electromechanical engineering from the University of Macau, Macau, China, in 2016, and the Ph.D. degree in electrical and computer engineering from the University of Macau, Macau, in 2021. He is currently an Assistant Professor with the Department of Automation, Shanghai Jiao Tong University, Shanghai, China. His research interests include nonlinear control of marine and aerial vehicles, coordinated control of multi-vehicle systems.

Pedro Casau, received the B.Sc. and M.Sc. degrees in aerospace engineering, and the Ph.D. degree (with distinction and Hons.) in electrical and computer engineering from Instituto Superior Tcnico (IST), Lisbon, Portugal, in 2008, 2010, and 2016, respectively. He is a Research Assistant with the SCORE Lab, Faculty of Science and Technology, University of Macau and a Junior Researcher with the Institute for Systems and Robotics, Lisbon, Portugal. While at IST, he participated on several national and international research projects on guidance, navigation and control of unmanned air vehicles (UAVs) and satellites. His current research interests include nonlinear control, hybrid control systems, vision-based control systems, controller design for autonomous air vehicles.

Carlos Silvestre, received the Licenciatura and masters degrees in electrical engineering, the Ph.D. degree in control science, and the Habilitation degree in electrical engineering and computers from the Instituto Superior Tcnico (IST), Lisbon, Portugal, in 1987, 1991, 2000, and 2011, respectively. Since 2000, he has been with the Department of Electrical Engineering, IST, where he is currently on leave. Since 2015, he has been a Professor with the Department of Electrical and Computer Engineering, Faculty of Science and Technology, University of Macau, Macau, China. His current research interests include linear and nonlinear control theory, hybrid systems, multiagent control systems, networked control systems, inertial navigation systems, and real-time architectures for complex autonomous systems with application to unmanned air and underwater vehicles.

Pedro Batista, received the Licenciatura degree in electrical and computer engineering, in 2005, and the Ph.D. degree, in 2010, both from the Instituto Superior Tcnico (IST), Lisbon, Portugal. From 2004 to 2006, he was a Monitor with the Department of Mathematics, IST. Since 2012, he has been with the Department of Electrical and Computer Engineering of IST, where he is currently an Assistant Professor with the Department of Electrical and Computer Engineering at IST. His research interests include sensor-based navigation and control of autonomous vehicles. Dr. Batista has received the Diploma de Mrito twice during his graduation and his Ph.D. thesis was awarded the Best Robotics Ph.D. Thesis Award by the Portuguese Society of Robotics.

Paulo Oliveira, received the Licenciatura, M.S., and Ph.D. degrees in electrical and computer engineering, and the Habilitation in mechanical engineering from the Instituto Superior Tecnico (IST), Lisbon, Portugal, in 1991, 2002, and 2016, respectively. He is an Associate Professor with the Department of Mechanical Engineering of IST and Senior Researcher with the Associated Laboratory for Energy, Transports, and Aeronautics. He is the author or coauthor of more than 65 journal papers and 175 conference communications and participated in more than 30 European and Portuguese research projects, over the last 30 years. His research interests include autonomous robotic vehicles with a focus on the fields of estimation,

sensor fusion, navigation, positioning, and mechatronics.

References

Aguiar, A. P., & Hespanha, J. P. (2007). Trajectory-tracking and path-following of underactuated autonomous vehicles with parametric modeling uncertainty. *IEEE Transactions on Automatic Control*, *52*(8), 1362–1379.

Barrau, A., & Bonnabel, S. (2017). The invariant extended kalman filter as a stable observer. *IEEE Transactions on Automatic Control*, *62*(4), 1797-1812.

Batista, P., Silvestre, C., & Oliveira, P. (2011). Single range aided navigation and source localization: Observability and filter design. *Systems & Control Letters*, *60*(8), 665-673. Retrieved from `https://www.sciencedirect.com/science/article/pii/S0167691111001174`

Benrezki, R. R., Tayebi, A., & Tadjine, M. (2018). Adaptive trajectory tracking control for vtol-uavs with unknown inertia, gyro-bias, and actuator loe. *International Journal of Robust and Nonlinear Control*, *28*(17), 5247-5261. Retrieved from `https://onlinelibrary.wiley.com/doi/abs/10.1002/rnc.4308`

Bouabdallah, S., & Siegwart, R. (2005). Backstepping and sliding-mode techniques applied to an indoor micro Quadrotor. In *Proceedings - ieee international conference on robotics and automation.*

Brockett, R. W., et al. (1983). Asymptotic stability and feedback stabilization. *Differential geometric control theory*, *27*(1), 181–191.

Bucy, R. S., & Joseph, P. D. (1968). *Filtering for stochastic processes with applications to guidance.* Interscience Publishers.

Cabecinhas, D., Batista, P., Oliveira, P., & Silvestre, C. (2018, May). Hovercraft control with dynamic parameters identification. *IEEE Transactions on Control Systems Technology*, *26*(3), 785-796.

Cabecinhas, D., Cunha, R., & Silvestre, C. (2014). A nonlinear quadrotor trajectory tracking controller with disturbance rejection. *Control Engineering Practice*, *26*, 1 - 10.

Castillo, P., Lozano, R., & Dzul, A. (2005). Stabilization of a mini rotorcraft with four rotors. *IEEE Control Systems Magazine*, *25*(6), 45-55.

Delyon, B. (2001). A note on uniform observability. *IEEE Transactions on Automatic Control*, *46*(8), 1326-1327.

Dydek, Z. T., Annaswamy, A. M., & Lavretsky, E. (2013, July). Adaptive control of quadrotor uavs: A design trade study with flight evaluations. *IEEE Transactions on Control Systems Technology*, *21*(4), 1400-1406.

Fang, Z., & Gao, W. (2012). Adaptive backstepping control of an indoor micro-quadrotor. *Research Journal of Applied Sciences, Engineering and Technology*, *4*(21), 4216–4226.

Hashim, H. A., Abouheaf, M., & Abido, M. A. (2021). Geometric stochastic filter with guaranteed performance for autonomous navigation based on imu and feature sensor fusion. *Control Engineering Practice*, *116*, 104926. Retrieved from `https://www.sciencedirect.com/science/article/pii/S0967066121002033`

Hoffmann, G., Huang, H., Waslander, S., & Tomlin, C. (2007). Quadrotor helicopter flight dynamics and control: Theory and experiment. In *Aiaa guidance, navigation and control conference and exhibit.*

Horn, R. A., & Johnson, C. R. (2012). *Matrix analysis* (2nd ed.). Cambridge University Press.

Hua, M.-D., & Allibert, G. (2018). Riccati observer design for pose, linear velocity and gravity direction estimation using landmark position and imu measurements. In *2018 ieee conference on control technology and applications (ccta)* (p. 1313-1318).

Huang, M., Xian, B., Diao, C., Yang, K., & Feng, Y. (2010, June). Adaptive tracking control of underactuated quadrotor unmanned aerial vehicles via backstepping. In *Proceedings of the 2010 american control conference* (p. 2076-2081).

Islam, S., Liu, P. X., & El Saddik, A. (2014, Oct 01). Nonlinear adaptive control for quadrotor flying vehicle. *Nonlinear Dynamics*, *78*(1), 117–133. Retrieved from https://doi.org/10.1007/s11071-014-1425-y

Jazwinski, A. H. (1970). *Stochastic processes and filtering theory.* New York, NY: Academic Press.

Kalman, R. E., & Bucy, R. S. (1961, 03). New Results in Linear Filtering and Prediction Theory. *Journal of Fluids Engineering*, *83*(1), 95-108.

Kamen, E. W., & Su, J. K. (1999). *Introduction to optimal estimation.* Springer Science & Business Media.

Khalil, H. K. (2002). *Nonlinear systems* (3rd ed ed.). Prentice Hall.

Lee, D., Kim, H. J., & Sastry, S. (2009). Feedback linearization vs. adaptive sliding mode control for a quadrotor helicopter. *International Journal of Control, Automation and Systems*.

Madani, T., & Benallegue, A. (2006). Backstepping control for a quadrotor helicopter. In *Ieee international conference on intelligent robots and systems.*

Maybeck, P. S. (1979). *Stochastic models, estimation, and control* (Vol. 1). Academic press.

Mellinger, D., Lindsey, Q., Shomin, M., & Kumar, V. (2011, Sep.). Design, modeling, estimation and control for aerial grasping and manipulation. In *2011 ieee/rsj international conference on intelligent robots and systems* (p. 2668-2673).

Mukherjee, P., & Waslander, S. L. (2012). Direct adaptive feedback linearization for quadrotor control. *AIAA Guidance, Navigation, and Control Conference 2012*.

Oriolo, G., & Nakamura, Y. (1991). Control of mechanical systems with second-order nonholonomic constraints: Underactuated manipulators. *Proceedings of the IEEE Conference on Decision and Control*, *3*, 2398–2403.

Pounds, P. E. I., Bersak, D. R., & Dollar, A. M. (2012, Aug 01). Stability of small-scale uav helicopters and quadrotors with added payload mass under pid control. *Autonomous Robots*, *33*(1), 129–142.

Sensor based Cooperative Robotics Research (SCORE) laboratory, at the Department of Electrical and Computer Engineering of the Faculty of Science and Technology, University of Macau. http://score.fst.umac.mo/. (2018).

Slotine, J.-J. E., Li, W., et al. (1991). *Applied nonlinear control* (Vol. 199) (No. 1). Prentice hall Englewood Cliffs, NJ.

Vicon Motion Systems Ltd. https://www.vicon.com/. (2018).

Viegas, D., Batista, P., Oliveira, P., & Silvestre, C. (2016). On the stability of the continuous-time kalman filter subject to exponentially decaying perturbations. *Systems & Control Letters*, *89*, 41 - 46.

Wang, C., Nahon, M., & Trentini, M. (2014, May). Controller development and validation for a small quadrotor with compensation for model variation. In *2014 international conference on unmanned aircraft systems (icuas)* (p. 902-909).

Wang, C., Song, B., Huang, P., & Tang, C. (2016, Aug 01). Trajectory tracking control for quadrotor robot subject to payload variation and wind gust disturbance. *Journal of Intelligent & Robotic Systems*, *83*(2), 315–333. Retrieved from https://doi.org/10.1007/s10846-016-0333-4

Weyl, H. (1912). Das asymptotische verteilungsgesetz der eigenwerte linearer partieller differentialgleichungen (mit einer anwendung auf die theorie der hohlraumstrahlung). *Mathematische Annalen*, *71*, 441-479.

Xie, W., Cabecinhas, D., Cunha, R., & Silvestre, C. (2019, Sep.). Robust motion control of an underactuated hovercraft. *IEEE Transactions on Control Systems Technology*, *27*(5), 2195-2208.

Xie, W., Yu, G., Cabecinhas, D., Cunha, R., & Silvestre, C. (2021). Global saturated tracking control of a quadcopter with experimental validation. *IEEE Control Systems Letters*, *5*(1), 169-174.

Xu, R., & Özgüner, Ü. (2006). Sliding mode control of a quadrotor helicopter. In *Proceedings of the ieee conference on decision and control.*

Zeng, W., Xian, B., Diao, C., Yin, Q., Li, H., & Yang, Y. (2011, Sep.). Nonlinear adaptive regulation control of a quadrotor unmanned aerial vehicle. In *2011 ieee international conference on control applications (cca)* (p. 133-138).

Appendix A. Proof of Lemma 2.2

Proof. To obtain the desired conclusion, it would suffice to ensure that the estimation error $\widetilde{\boldsymbol{\zeta}}$ in (9) converges globally exponentially to the origin. This is true if the pair $(\mathbf{A}_{\boldsymbol{\zeta}}, \mathbf{C}_{\boldsymbol{\zeta}})$ is UCO, in light of (Jazwinski, 1970, Theorem 7.4) and (Bucy & Joseph, 1968, Theorem 5.4). Then, we just need to show that $(\mathbf{A}_{\boldsymbol{\zeta}}, \mathbf{C}_{\boldsymbol{\zeta}})$ is UCO. The arguments in the sequel resemble those of (Batista et al., 2011, Theorem 4). Given the structure of $\boldsymbol{\Phi}$ in (7), we obtain

$$\begin{aligned}\mathbf{W}(t, t+\Delta t) &= \int_t^{t+\Delta t} \boldsymbol{\Phi}^\top(\tau, t)\mathbf{C}_{\boldsymbol{\zeta}}^\top \mathbf{R}_{\boldsymbol{\zeta}}^{-1}\mathbf{C}_{\boldsymbol{\zeta}}\boldsymbol{\Phi}(\tau, t)d\tau \\ &= \int_t^{t+\Delta t} [\mathbf{I}_n \int_t^\tau \mathbf{A}_{\boldsymbol{\xi}}(\sigma)d\sigma]^\top \mathbf{R}_{\boldsymbol{\zeta}}^{-1}[\mathbf{I}_n \int_t^\tau \mathbf{A}_{\boldsymbol{\xi}}(\sigma)d\sigma]d\tau.\end{aligned} \tag{A1}$$

Then the quadratic form $\mathbf{d}^\top \mathbf{W}(t, t+\Delta t)\mathbf{d}$ in Definition 2.1 with a unit vector $\mathbf{d} \in \mathbb{R}^{n+m}$ is computed as

$$\mathbf{d}^\top \mathbf{W}(t, t+\Delta t)\mathbf{d} = \int_t^{t+\Delta t} \left\| \mathbf{R}_{\boldsymbol{\zeta}}^{-1/2} \left[\mathbf{I}_n \quad \textstyle\int_t^\tau \mathbf{A}_{\boldsymbol{\xi}}(\sigma)d\sigma\right] \mathbf{d} \right\|^2 d\tau. \tag{A2}$$

Since $\mathbf{W}(t, t+\Delta t)$ is a definite integral of continuous bounded functions of time, for every chosen $\Delta t \in \mathbb{R}_{>0}$, there exists a $\chi \in \mathbb{R}_{>0}$ that satisfies the right-hand side of (11) for every $t \geq t_0$ and every unit vector $\mathbf{d} \in \mathbb{R}^{n+m}$. Consider a partition of an arbitrary unit vector $\mathbf{d} = [\mathbf{d}_1^\top \ \mathbf{d}_2^\top]^\top$ with $\mathbf{d}_1 \in \mathbb{R}^n$ and $\mathbf{d}_2 \in \mathbb{R}^m$. If $\mathbf{d}_1 \neq \mathbf{0}_{n\times 1}$, then

$$\left\| \mathbf{R}_{\boldsymbol{\zeta}}^{-1/2} \left[\mathbf{I}_n \quad \textstyle\int_t^t \mathbf{A}_{\boldsymbol{\xi}}(\sigma)d\sigma\right] \mathbf{d} \right\| = \left\| \mathbf{R}_{\boldsymbol{\zeta}}^{-1/2}\mathbf{d}_1 \right\| > 0 \tag{A3}$$

for every $t \geq t_0$. An application of (Batista et al., 2011, Proposition 2) leads to the existence of $\chi_1, \Delta t_1 \in \mathbb{R}_{>0}$ satisfying

$$\mathbf{d}^\top \mathbf{W}(t, t+\Delta t_1)\mathbf{d} \geq \chi_1 \tag{A4}$$

for every $t \geq t_0$ and for every unit vector $\mathbf{d}$. If $\mathbf{d}_1 = \mathbf{0}_{n\times 1}$, then (A2) can be rewritten as

$$\mathbf{d}^\top \mathbf{W}(t, t+\Delta t)\mathbf{d} = \int_t^{t+\Delta t} \left\| \mathbf{R}_{\boldsymbol{\zeta}}^{-1/2} \int_t^\tau \mathbf{A}_{\boldsymbol{\xi}}(\sigma)\mathbf{d}_2 d\sigma \right\|^2 d\tau, \tag{A5}$$

whose integrand is positive due to the inequality (12) by letting $\mathbf{d}_2 = \mathbf{c}$. Applying (Batista et al., 2011, Proposition 2) again gives $\chi_2 \in \mathbb{R}_{>0}$ and $\Delta t_2 \in (0, \tau]$ that satisfy

$$\mathbf{d}^\top \mathbf{W}(t, t+\Delta t_2)\mathbf{d} \geq \chi_2 \tag{A6}$$

for every $t \geq t_0$. Choosing χ large enough such that $\chi^{-1} \leq \min\{\chi_1, \chi_2\}$, we conclude that $(\mathbf{A}_{\boldsymbol{\zeta}}, \mathbf{C}_{\boldsymbol{\zeta}})$ is UCO holds true, which implies global exponential convergence of the estimate $\widehat{\boldsymbol{\zeta}}$ of the Kalman-Bucy filter (8) to the state $\boldsymbol{\zeta}$ of the system (6). □

Appendix B. Proof of Lemma 2.5

By (16), we have the following statements:

$$\exists T_1 > 0 \, \forall t \geq T_1, \sigma_1(t) = \Sigma_1, \tag{B1}$$
$$\exists T_2 > 0 \, \forall t \geq T_2, \widetilde{\sigma}_2(t) \leq \theta_2 \Sigma_2, \tag{B2}$$
$$\forall \epsilon > 0 \, \exists T_3 > 0 \, \forall t \geq T_3, \sigma_3(t) \leq \epsilon, \tag{B3}$$

where $\theta_i \in (0,1)$ for each $i \in \{1,2,3\}$ and $\widetilde{\sigma}_2 : \mathbb{R}_{\geq 0} \to \mathbb{R}$ defined by $\widetilde{\sigma}_2(t) = \sigma_2(t) - \Sigma_2$. Hence, (15) can be rewritten as

$$\begin{aligned} U(\mathbf{x}, t) = &- \left(1 - \sum_{i=1}^{3} \theta_i\right) \Sigma_2 \|\mathbf{x}\|^2 \\ &- (\theta_1 \Sigma_2 \|\mathbf{x}\| - \Sigma_1) \|\mathbf{x}\| - (\theta_2 \Sigma_2 + \widetilde{\sigma}_2(t)) \|\mathbf{x}\|^2 - (\theta_3 \Sigma_2 - \sigma_3 \|\mathbf{x}\|) \|\mathbf{x}\|^3 \end{aligned} \tag{B4}$$

for every $t \geq T_1$. Select $T = \max\{T_1, T_2, T_3\} > 0$, $c = \left(1 - \sum_{i=1}^{3} \theta_i\right) \Sigma_2 > 0$, $a = \Sigma_1 \theta_1^{-1} \Sigma_2^{-1} > 0$, $b = \theta_3 \Sigma_2 \epsilon^{-1} > 0$, we have that

$$U(\mathbf{x}, t) \leq -c \|\mathbf{x}\|^2 \tag{B5}$$

for every $t \geq T$ and for every $\mathbf{x}$ such that $a \leq \|\mathbf{x}\| \leq b$. Note that ϵ can be made sufficiently small to satisfy $a < b$.

Appendix C. Proof of Lemma 4.2

Proof. We summarize the error dynamics driven by control laws defined in (38) and (44) as

$$\begin{aligned} \dot{\mathbf{z}}_1(\mathbf{z}_1, \mathbf{z}_2, t) &= -k_1 \mathbf{z}_1 + \mathbf{R}(t)(\mathbf{z}_2 + \boldsymbol{\delta}), \\ \dot{\mathbf{z}}_2(\mathbf{z}, t) &= -k_2 \mathbf{z}_2 + \mathbf{S}(\boldsymbol{\delta}) \mathbf{z}_3 + \mathbf{S}(\mathbf{z}_2) \boldsymbol{\omega}, \\ \dot{\mathbf{z}}_3(\mathbf{z}_2, \mathbf{z}_3) &= -k_3 \mathbf{z}_3 + \beta^{-1} \mathbf{S}(\boldsymbol{\delta}) \mathbf{z}_2, \end{aligned} \tag{C1}$$

where $\mathbf{z} := [\mathbf{z}_1^\top \ \mathbf{z}_2^\top \ \mathbf{z}_3^\top]^\top$ and $\boldsymbol{\omega}$ can be written in terms of $\mathbf{z}$, $\mathbf{R}$, $\ddot{\mathbf{p}}_d$, and t in virtue of (39). We first study the system above by examining the Lyapunov candidate function given in (42), rewritten as

$$V_3(\mathbf{z}) := \frac{1}{2} \alpha \mathbf{z}_1^\top \mathbf{z}_1 + \frac{1}{2} \mathbf{z}_2^\top \mathbf{z}_2 + \frac{1}{2} \beta \mathbf{z}_3^\top \mathbf{z}_3 \tag{C2}$$

for every $\mathbf{z} \in \mathbb{R}^9$, where $\alpha \in (0, 4k_1k_2)$, with its time derivative along the solution to (C1), given in (45), rewritten as

$$\begin{aligned}\dot{V}_3(\mathbf{z},t) =& -\alpha k_1 \mathbf{z}_1^\top \mathbf{z}_1 - k_2 \mathbf{z}_2^\top \mathbf{z}_2 - \beta k_3 \mathbf{z}_3^\top \mathbf{z}_3 + \alpha \mathbf{z}_1^\top \mathbf{R}(t)(\mathbf{z}_2 + \boldsymbol{\delta}) \\ \leq& -\lambda_3(\mathbf{K}) \|\mathbf{z}\|^2 + \alpha \|\boldsymbol{\delta}\| \|\mathbf{z}\| \\ \leq& -(1-\theta)\lambda_3(\mathbf{K}) \|\mathbf{z}\|^2, \forall \|\mathbf{z}\| \geq \theta^{-1}\lambda_3^{-1}(\mathbf{K})\alpha \|\boldsymbol{\delta}\|,\end{aligned} \tag{C3}$$

where the matrix

$$\mathbf{K} := \begin{bmatrix} \alpha k_1 & -\frac{1}{2}\alpha & 0 \\ -\frac{1}{2}\alpha & k_2 & 0 \\ 0 & 0 & \beta k_3 \end{bmatrix} \tag{C4}$$

is positive definite and $\theta \in (0,1)$. By (Khalil, 2002, Theorem 4.18), the solution to (C1) exists and is uniformly bounded for every $t \in \mathbb{R}_{\geq 0}$. Next, we study the $(\mathbf{z}_2, \mathbf{z}_3)$-subsystem. Consider the Lyapunov candidate function

$$V_4(\mathbf{z}_2, \mathbf{z}_3) := \frac{1}{2}\mathbf{z}_2^\top \mathbf{z}_2 + \frac{1}{2}\beta \mathbf{z}_3^\top \mathbf{z}_3 \tag{C5}$$

for every $[\mathbf{z}_2^\top \ \mathbf{z}_3^\top]^\top \in \mathbb{R}^6$, whose time derivative along the solution to the $(\mathbf{z}_2, \mathbf{z}_3)$-subsystem in (C1) is

$$\dot{V}_4(\mathbf{z}_2, \mathbf{z}_3) = -k_2 \mathbf{z}_2^\top \mathbf{z}_2 - \beta k_3 \mathbf{z}_3^\top \mathbf{z}_3, \tag{C6}$$

from which we conclude global exponential stability for the origin of the $(\mathbf{z}_2, \mathbf{z}_3)$-subsystem in (C1) by (Khalil, 2002, Theorem 4.10). Finally, consider the Lyapunov candidate function (27), whose time derivative along the solution to $\mathbf{z}_1$-subsystem in (C1), driven by input $\mathbf{z}_2$, is

$$\begin{aligned}&\dot{V}_1(\mathbf{z}_1, \mathbf{z}_2, t) = -\alpha k_1 \mathbf{z}_1^\top \mathbf{z}_1 + \alpha \mathbf{z}_1^\top \mathbf{R}(t)(\mathbf{z}_2 + \boldsymbol{\delta}) \\ &\leq -\frac{1}{2}\alpha k_1 \|\mathbf{z}_1\|^2 - \alpha \|\mathbf{z}_1\| \left(\frac{1}{2}k_1 \|\mathbf{z}_1\| - \|\mathbf{z}_2\| - \|\boldsymbol{\delta}\|\right) \\ &\leq -\frac{1}{2}\alpha k_1 \|\mathbf{z}_1\|^2, \forall \|\mathbf{z}_1\| \geq 2k_1^{-1}(\|\mathbf{z}_2\| + \|\boldsymbol{\delta}\|).\end{aligned} \tag{C7}$$

The stated conclusion on the uniform ultimate unboundedness of $\mathbf{z}_1$ follows from (Khalil, 2002, Theorem 4.19), by noticing that $\mathbf{z}_2(t) \to 0$ as $t \to \infty$. By (29), (39), (38), and (44), we conclude that $\mathbf{v}$, $\boldsymbol{\omega}$, T, and $\boldsymbol{\tau}$ are bounded on $\mathbb{R}_{\geq 0}$. □

Appendix D. Proof of Theorem 6.1

Proof. We summarize the error dynamics driven by control laws defined in (56) and (57) as

$$\begin{aligned}\dot{\mathbf{z}}_1(\mathbf{z}_1,\mathbf{z}_2,t) &= -k_1\mathbf{z}_1 + \mathbf{R}(t)(\mathbf{z}_2+\boldsymbol{\delta}),\\ \dot{\mathbf{z}}_2(\widehat{\mathbf{z}},t,\widetilde{\boldsymbol{\xi}},\widetilde{\boldsymbol{\eta}}) &= -k_2\mathbf{z}_2 + \mathbf{S}(\boldsymbol{\delta})\widehat{\mathbf{z}}_3 + \mathbf{S}(\mathbf{z}_2)\boldsymbol{\omega} + \mathbf{f}(\mathbf{z}_1,\mathbf{z}_2,t,\widetilde{\boldsymbol{\xi}},\widetilde{\boldsymbol{\eta}}),\\ \dot{\widehat{\mathbf{z}}}_3(\widehat{\mathbf{z}},t,\widetilde{\boldsymbol{\xi}},\widetilde{\boldsymbol{\eta}},\dot{\widetilde{\boldsymbol{\xi}}}) &= -k_3\widehat{\mathbf{z}}_3 + \beta^{-1}\mathbf{S}(\boldsymbol{\delta})\mathbf{z}_2 + \mathbf{g}(\widehat{\mathbf{z}},t,\widetilde{\boldsymbol{\xi}},\widetilde{\boldsymbol{\eta}},\dot{\widetilde{\boldsymbol{\xi}}}),\end{aligned} \tag{D1}$$

where $\widehat{\mathbf{z}} := [\mathbf{z}_1^\top\ \mathbf{z}_2^\top\ \widehat{\mathbf{z}}_3^\top]^\top$, and $\boldsymbol{\omega}$ can be written in terms of $\widehat{\mathbf{z}}$, $\mathbf{R}$, $\ddot{\mathbf{p}}_d$, $\widehat{\boldsymbol{\xi}}$, and t. The functions $\mathbf{f}$ and $\mathbf{g}$ are error terms induced by using estimates of parameters rather than their actual values but satisfy

$$\|\mathbf{f}(\mathbf{z}_1,\mathbf{z}_2,t,\widetilde{\boldsymbol{\xi}},\widetilde{\boldsymbol{\eta}})\| \le \sum_{i=0}^{1}\rho_{f,i}(\widetilde{\boldsymbol{\xi}},\widetilde{\boldsymbol{\eta}})\|\widehat{\mathbf{z}}\|^i, \quad \|\mathbf{g}(\widehat{\mathbf{z}},t,\widetilde{\boldsymbol{\xi}},\widetilde{\boldsymbol{\eta}},\dot{\widetilde{\boldsymbol{\xi}}})\| \le \sum_{j=0}^{2}\rho_{g,j}(\widetilde{\boldsymbol{\xi}},\widetilde{\boldsymbol{\eta}})\|\widehat{\mathbf{z}}\|^j \tag{D2}$$

for every $(\widehat{\mathbf{z}},t,\widetilde{\boldsymbol{\xi}},\widetilde{\boldsymbol{\eta}},\dot{\widetilde{\boldsymbol{\xi}}}) \in \mathbb{R}^9\times\mathbb{R}_{\ge0}\times\mathbb{R}^{10}\times\mathbb{R}^4\times\mathbb{R}^{10}$, where each function $\rho_{f,i}$ and $\rho_{g,j}$ is non-negative with respect to its arguments. Now consider the Lyapunov candidate function in the same form as (C2), defined as

$$\widehat{V}_3(\widehat{\mathbf{z}}) := \frac{1}{2}\alpha\mathbf{z}_1^\top\mathbf{z}_1 + \frac{1}{2}\mathbf{z}_2^\top\mathbf{z}_2 + \frac{1}{2}\beta\widehat{\mathbf{z}}_3^\top\widehat{\mathbf{z}}_3 \tag{D3}$$

for every $\widehat{\mathbf{z}} \in \mathbb{R}^9$, where $\alpha \in (0, 4k_1k_2)$ plays the same role as in the proof of Lemma 4.2. Lengthy but straightforward computations show that the time derivative of (D3) along the solution to (D1) satisfies

$$\begin{aligned}\dot{\widehat{V}}_3(\widehat{\mathbf{z}},t) &= -\alpha k_1\mathbf{z}_1^\top\mathbf{z}_1 - k_2\mathbf{z}_2^\top\mathbf{z}_2 - \beta k_3\widehat{\mathbf{z}}_3^\top\widehat{\mathbf{z}}_3 + \alpha\mathbf{z}_1^\top\mathbf{R}(t)(\mathbf{z}_2+\boldsymbol{\delta})\\ &\quad + \mathbf{z}_2^\top\mathbf{f}(\mathbf{z}_1(t),\mathbf{z}_2(t),t,\widetilde{\boldsymbol{\xi}}(t),\widetilde{\boldsymbol{\eta}}(t)) + \beta\widehat{\mathbf{z}}_3^\top\mathbf{g}(\widehat{\mathbf{z}}(t),t,\widetilde{\boldsymbol{\xi}}(t),\widetilde{\boldsymbol{\eta}}(t),\dot{\widetilde{\boldsymbol{\xi}}}(t))\\ &\le -\sigma_2(t)\,\|\widehat{\mathbf{z}}\|^2 + \sigma_1(t)\,\|\widehat{\mathbf{z}}\| + \sigma_3(t)\,\|\widehat{\mathbf{z}}\|^3\end{aligned} \tag{D4}$$

for every $t \in \mathbb{R}_{\ge0}$. For simpler presentation of the functions σ_1, σ_2, and σ_3, we introduce the function

$$s_{\mathbf{C},n}(x,y) := \sum_{i,j\in\{1,2,\ldots,n+1\}} c_{ij}x^{i-1}y^{j-1} \tag{D5}$$

to denote the $2n$-th order bivariate polynomial in $x \in \mathbb{R}$ and $y \in \mathbb{R}$ with non-negative coefficient $c_{ij} \in \mathbb{R}_{\ge0}$ being the entry of $\mathbf{C} \in \mathbb{R}^{(n+1)\times(n+1)}$ on the i-th row and j-th column, while $c_{11} = 0$. Using such notation, we present the following definitions (time dependence is omitted):

$$\begin{aligned}\sigma_1 &:= 3\sup\{\alpha\|\boldsymbol{\delta}\|, s_{\mathbf{C}_1,1}(\|\widetilde{\boldsymbol{\xi}}\|,\|\widetilde{\boldsymbol{\eta}}\|), s_{\mathbf{C}_2,3}(\|\widetilde{\boldsymbol{\xi}}\|,\|\widetilde{\boldsymbol{\eta}}\|)\},\\ \sigma_2 &:= \lambda_3(\mathbf{K}) + \lambda_3(\widetilde{\mathbf{K}}),\\ \sigma_3 &:= 6\sup_{i\in\{8,9,10,11,12,13\}} s_{\mathbf{C}_i,1}(\|\widetilde{\boldsymbol{\xi}}\|,\|\widetilde{\boldsymbol{\eta}}\|),\end{aligned} \tag{D6}$$

where $\mathbf{K}$ is defined in (C4) and

$$\widetilde{\mathbf{K}} := \begin{bmatrix} 0 & -\kappa_{12} & -\kappa_{13} \\ -\kappa_{12} & \kappa_2 & -\kappa_{23} \\ -\kappa_{13} & -\kappa_{23} & \kappa_3 \end{bmatrix} \tag{D7}$$

with $\kappa_2 := s_{\mathbf{C}_3,1}(\|\widetilde{\boldsymbol{\xi}}\|, \|\widetilde{\boldsymbol{\eta}}\|)$, $\kappa_3 := s_{\mathbf{C}_4,2}(\|\widetilde{\boldsymbol{\xi}}\|, \|\widetilde{\boldsymbol{\eta}}\|)$, $\kappa_{12} := s_{\mathbf{C}_5,2}(\|\widetilde{\boldsymbol{\xi}}\|, \|\widetilde{\boldsymbol{\eta}}\|)$, $\kappa_{13} := s_{\mathbf{C}_6,2}(\|\widetilde{\boldsymbol{\xi}}\|, \|\widetilde{\boldsymbol{\eta}}\|)$, and $\kappa_{23} := s_{\mathbf{C}_7,2}(\|\widetilde{\boldsymbol{\xi}}\|, \|\widetilde{\boldsymbol{\eta}}\|)$. We remark here that, to obtain the expression of σ_2, Lemma 2.3 is invoked in the deduction of (D4), namely $\lambda_3(\mathbf{K} + \widetilde{\mathbf{K}}) \geq \lambda_3(\mathbf{K}) + \lambda_3(\widetilde{\mathbf{K}})$.

Since Assumption 2 holds, it follows from Lemma 2.2 that the estimators for $\boldsymbol{\xi}$ and $\boldsymbol{\eta}$ are exponentially stable. By Lemma 2.4, the eigenvalues of a matrix depend continuously on the entries of the matrix. Then it follows from continuity of $\widetilde{\mathbf{K}}$ that $\lambda_3(\widetilde{\mathbf{K}})$ is a continuous function of t. Since each entry of $\widetilde{\mathbf{K}}$ converges to 0 as time approaches infinity, $\lambda_3(\widetilde{\mathbf{K}})$ also converges to 0 as time approaches infinity. We are now in the condition of Lemma 2.5 where $\Sigma_1 = \alpha\|\boldsymbol{\delta}\|$ and $\Sigma_2 = \lambda_3(\mathbf{K})$, in view of (D6). A careful deduction reveals the existence of $T > 0$ such that

$$\dot{\widehat{V}}_3(\widehat{\mathbf{z}}, t) \leq -\left(1 - \sum_{i=1}^{3} \theta_i\right) \lambda_3(\mathbf{K}) \, \|\widehat{\mathbf{z}}\|^2 \tag{D8}$$

for every $t \geq T$ and every $\widehat{\mathbf{z}}$ such that $\theta_3^{-1}\lambda_3^{-1}(\mathbf{K})\alpha\|\boldsymbol{\delta}\| \leq \|\widehat{\mathbf{z}}\| \leq \theta_1\lambda_3(\mathbf{K})\epsilon^{-1}$, where $\theta_i \in (0, 1)$ for each $i \in \{1, 2, 3\}$ and $\epsilon > 0$ is picked to be sufficiently small. It follows from (Khalil, 2002, Theorem 4.18) that the solution to (D1) is uniformly ultimately bounded by $2\lambda_3^{-1}(\mathbf{K})\alpha\|\boldsymbol{\delta}\|$. □

Appendix E. Program for Checking the Premise of Lemma 2.2

Algorithm 1 Algorithm for checking the premise of Lemma 2.2

Input: $t \mapsto \boldsymbol{A}_{\boldsymbol{\xi}}(t)$ (extracted from simulations), MaxSam (maximum sampling time for numerical solvers), t_f (stopping time), AbsTol (absolute tolerance for numerical solvers)

Initialization: $t_0 = 0$, $\epsilon = 0.01$, $\Delta t \geq$ MaxSam

numerical integration $\mathbf{A}^i_{\boldsymbol{\xi}}(t_0, \Delta t) \approx \int_t^\tau \mathbf{A}_{\boldsymbol{\xi}}(\sigma) d\sigma$
solve for all $\mathbf{c}^\star \in \text{Null}\left(\mathbf{A}^i_{\boldsymbol{\xi}}(t_0, \Delta t)\right)$ on the unit sphere
for all $\mathbf{c}^\star$ **do**
  generate random sample $\mathbf{c}$ on the unit sphere near $\mathbf{c}^\star$
  while $\left\|\mathbf{A}^i_{\boldsymbol{\xi}}(t_0, \Delta t)\mathbf{c}\right\| \leq \epsilon$ and $t_0 + \Delta t \leq t_f$ **do**
    increase Δt
  end while
  return Δt
end for
find $\overline{\Delta} t$, the maximum of all Δt
repeat
  above procedures by increasing t_0 and record each $\overline{\Delta} t$
until $t_0 + \overline{\Delta} t \geq t_f/2$
find $\overline{\overline{\Delta}} t$, the maximum of all $\overline{\Delta} t$
if $\overline{\overline{\Delta}} t \leq t_f/2$ **then**
  print fulfillment of the premise of Lemma 2.2 with ϵ and $\Delta t = \overline{\overline{\Delta}} t$
else
  print violation of the premise of Lemma 2.2, try decreasing $\epsilon \geq$ AbsTol
end if